American Mineralogist, Volume 106, pages 1113–1127, 2021

Phase diagram and thermal expansion of orthopyroxene-, clinopyroxene-, and ilmenite-structured $MgGeO_3$

Simon A. Hunt[1,2,*], James R. Santangeli[2], David P. Dobson[2], and Ian G. Wood[2]

[1]Department of Materials, University of Manchester, Sackville Street Building, Manchester M1 3BB, U.K.
[2]Department of Earth Sciences, University College London, Gower Street, London WC1E 6BT, U.K.

Abstract

The $MgGeO_3$ system is a low-pressure analog for the Earth-forming $(Mg,Fe)SiO_3$ system and exhibits recoverable orthopyroxene, clinopyroxene, and ilmenite structures below 6 GPa. The pressure-temperature conditions of the clinopyroxene to ilmenite phase transition are reasonably consistent between studies, having a positive Clapeyron slope and occurring between 4 and 7 GPa in the temperature range 900–1600 K. There are, though, significant discrepancies in the Clapeyron slope of the orthopyroxene to clinopyroxene phase transition in existing works that also disagree on the stable phase at ambient conditions. The most significant factor in these differences is the method used; high-pressure experiments and thermophysical property measurements yield apparently contradicting results. Here, we perform both high pressure and temperature experiments as well as thermal expansion measurements to reconcile the measurements. High-pressure and -temperature experiments yield a Clapeyron slope of $-1.0^{+1.0}_{-0.7}$ MPa/K for the $MgGeO_3$ orthopyroxene-clinopyroxene phase transition, consistent with previous high-pressure and -temperature experiments. The $MgGeO_3$ orthopyroxene-clinopyroxene-ilmenite triple point is determined to be at 0.98 GPa and 752 K, with the ilmenite phase stable at ambient conditions. The high-temperature (>600 K) thermal expansion of the clinopyroxene phase is greater than that of the other phases. Debye-Grüneisen relationships fitted to the volume-temperature data give Debye temperatures for the orthopyroxene, clinopyroxene, and ilmenite phases of 602(7), 693(10), and 758(13) K and V_0 of 897.299(16), 433.192(10), and 289.156(6) Å^3, respectively. The Clapeyron slopes calculated directly from the Debye-Grüneisen relationships are consistent with previous thermophysical property measurements. The presence of significant anharmonicity and/or formation of defects in the clinopyroxene phase at high-temperatures, which is not apparent in the other phases, accounts for the previous contradictions between studies. The inferred increased heat capacity of the clinopyroxene corresponds to an increase in entropy and an expanded phase field at high temperatures.

Keywords: Equation of state, heat capacity, thermal expansion, high-pressure, high-temperature, phase transition, anharmonicity

Introduction

The MgO-GeO_2 system has long been studied because of its similarity to the MgO-SiO_2 system but with structure types stable at lower pressures. Like $MgSiO_3$, $MgGeO_3$ transforms from the ilmenite structure to both the perovskite structure (at around 12 GPa; Leinenweber et al. 1994) and the post-perovskite structure (around 65 GPa; Akaogi et al. 2005; Hirose et al. 2005). Below 10 GPa, $MgGeO_3$, like $MgSiO_3$, exhibits orthopyroxene, clinopyroxene, and ilmenite structures (Ringwood and Seabrook 1962; Kirfel and Neuhaus 1974; Ozima and Akimoto 1983; Ross and Navrotsky 1988). Both the MgO-GeO_2 and MgO-SiO_2 systems have ambient-pressure olivine structures that transform to spinel structures at elevated pressure and temperature (Ross and Navrotsky 1987; Akaogi et al. 1989). The germanate system is not, though, a perfect low-pressure reflection of the silicate system. Pure GeO_2 is stable in the rutile structure at ambient conditions and above 1310 K transforms to that of quartz (Laubengayer and Morton 1932). This contrasts with SiO_2, in which quartz is the ambient-pressure phase and the rutile structure is stable above 9 GPa as stishovite. These two silica phases are separated by coesite, which has not been found in GeO_2. Neither has the wadsleyite (β-Mg_2SiO_4) structure been observed in Mg_2GeO_4. Above about 4 GPa and 1000 K in $MgGeO_3$, the ilmenite structure is stable, and there is no appearance of the Mg_2SiO_4 + SiO_2 field that separates the clinopyroxene and ilmenite phases in the $MgSiO_3$ system. An additional intermediate phase occurs in the MgO-GeO_2 binary that is not present in the MgO-SiO_2 binary. Initially reported as Mg_4GeO_6 (Robbins and Levin 1959; McCormick 1964) and subsequently refined to be $Mg_{3.5}Ge_{1.25}O_6$ with space group *Pbam* (von Dreele et al. 1970; Kostiner and Bless 1971), at ambient pressure, it is stable below 1768 K, whereupon it breaks down to Mg_2GeO_4 + MgO (Robbins and Levin 1959).

There is more reported complexity in the silicate pyroxenes (e.g., Ohi and Miyake 2016) than in the germanate equivalents. Silicate clinopyroxene, with the space group *C*2/*c*, is stable above about 7 GPa (Ulmer and Stalder 2001). At low pressures, this transforms to either low-clinoenstatite (space group $P2_1/c$) or, above 1073 K, orthoenstatite (space group *Pbca*). Above ~1270 K, orthoenstatite transforms to an unrecoverable protoenstatite (space group *Pbcn*) (Murakami et al. 1982).

Only the orthoenstatite (*Pbca*) and high-clinopyroxene (*C*2/*c*)

* E-mail: simon.hunt@manchester.ac.uk. Orcid 000-0003-3817-8835

structures have been recovered in $MgGeO_3$, although the low-clinopyroxene form has been observed in other pyroxene-structured germanates (e.g., $LiFeGe_2O_6$; Redhammer et al. 2010b). At ambient pressure, Robbins and Levin (1959) report that orthopyroxene-$MgGeO_3$ transforms to a high-clinopyroxene structure ($C2/c$) above 1828 ± 5 K. They comment that it is possible that the high-clinopyroxene phase is the back-transformation product of a "proto-pyroxene" phase. This would be consistent with the $MgSiO_3$-$MgGeO_3$ binary that has the enstatite-protoenstatite transition temperature increasing from ~1310 to 1620 K between 0 and 12.5 mol% $MgGeO_3$ (Sarver and Hummel 1963). In addition, Lyon (1968) compared the observed diffraction peaks of the recovered high-temperature clinopyroxene phase unfavorably to the $C2/c$ space group but did not make or analyze the clinopyroxene himself. Ozima and Akimoto (1983) argued that protoenstatite is the stable $MgGeO_3$ phase above ~1200 K, but this is in disagreement with most other studies.

At pressures greater than ~4 GPa, $MgGeO_3$ adopts the ilmenite structure (Kirfel and Neuhaus 1974; Ozima and Akimoto 1983; Ross and Navrotsky 1988) (Fig. 1). The clinopyroxene-ilmenite phase boundary is at lower pressure in the study of Ross and Navrotsky (1988) but is conceivably within the systematic errors of the experiments.

There however remains disagreement between studies as to the phase diagram of $MgGeO_3$ below the ilmenite stability field. The extensive experimental study of Kirfel and Neuhaus (1974) proposed a negative Clapeyron slope for the orthopyroxene-clinopyroxene phase boundary with orthopyroxene as the low-temperature–low-pressure phase (Fig. 1a). This is topologically consistent with Ringwood and Seabrook (1962) who, though, synthesized the clinopyroxene phase at 0.5 GPa. They therefore questioned whether the shallowness of the phase boundary was caused by shear stresses rather than pressure, as has been observed in natural pyroxenes (Coe and Kirby 1975). Yamanaka et al. (1985) transformed pre-synthesized clinopyroxene phase to orthopyroxene phase at ~1173 K and ambient pressure and attempted, but did not observe, the reverse orthopyroxene to clinopyroxene phase reaction at 973 K and ambient pressure. The phase boundaries of Kirfel and Neuhaus (1974) are consistent with the high-pressure and temperature experimental constraints of Ross and Navrotsky (1988) (Fig. 1b) but not with the positive Clapeyron slope derived by calorimetric measurements. The calorimetric Clapeyron slope makes the clinopyroxene phase the low-temperature–low-pressure phase and the stable phase at ambient conditions. Interestingly, the reported experimental results of both Kirfel and Neuhaus (1974) and Ross and Navrotsky (1988) are consistent with the reported sample synthesis conditions of all other studies (Roth 1955; Ringwood and Seabrook 1962; Liebermann 1974; Sato et al. 1977; Kirfel et al. 1978; Ito and Matsui 1979; Ashida et al. 1985; Okada et al. 2008) (Fig. 1b) except that of Ozima and Akimoto (1983) (Fig. 1c).

Ozima and Akimoto (1983) grew orthopyroxene phase and two types of clinopyroxene $MgGeO_3$ crystals from flux at ambient pressure. They argued that clinopyroxene is the low temperature phase, which transforms to ortho- and the proto-pyroxene structures with increasing temperature. They also reported the stability of orthopyroxene phase between 3 and 5 GPa and ~1300 K where all other authors report the clinopyroxene phase.

Only a few measurements of the thermophysical properties of $MgGeO_3$ phases have been made. Ross and Navrotsky (1988) used high-temperature solution calorimetry and room-temperature vibrational spectroscopy measurements of the three phases that they amalgamated to produce a thermodynamically consistent phase diagram (Fig. 1b). Yamanaka et al. (1985) measured the thermal expansion and thermal evolution of the crystal structures of the ortho- and clinopyroxene phases between

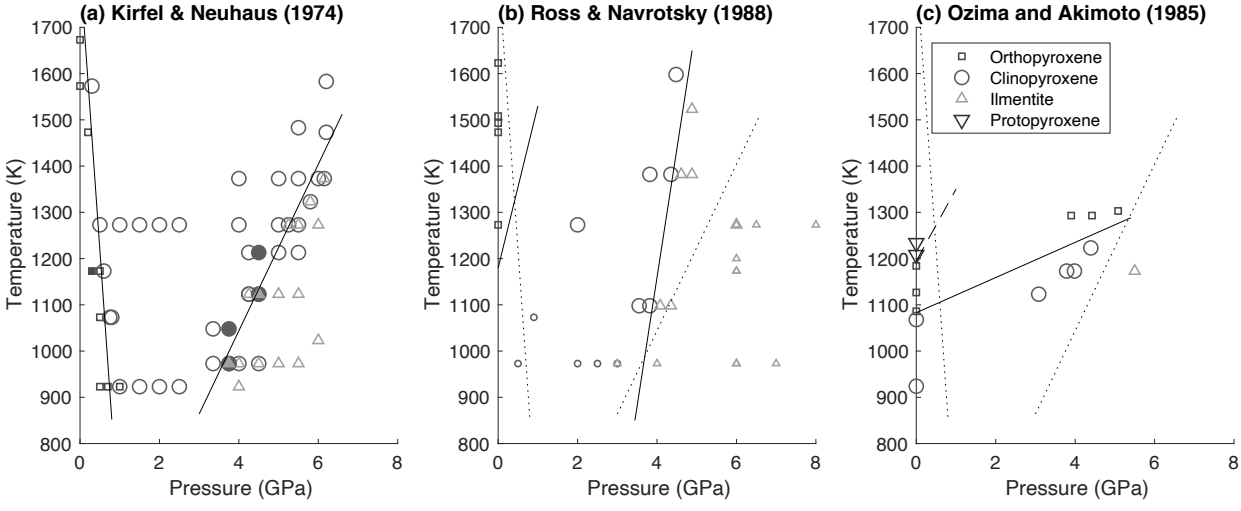

Figure 1. Phase diagrams and synthesis conditions in the $MgGeO_3$ system from previous studies. Large symbols are data from (**a**) Kirfel and Neuhaus (1974), (**b**) Ross and Navrotsky (1988), and (**c**) Ozima and Akimoto (1983). Small symbols in **b** are synthesis conditions reported by Roth (1955); Ringwood and Seabrook (1962); Liebermann (1974); Sato et al. (1977); Kirfel et al. (1978); Ito and Matsui (1979); Ashida et al. (1985); Okada et al. (2008). Symbols: square = orthopyroxene, circle = clinopyroxene, upward-pointing triangle = ilmenite, downward-pointing triangle = protopyroxene; open = forward and filled = reversals, except data of Ross and Navrotsky (1988) (**b**) where all experiments started with both clinopyroxene and ilmenite so are both forward and reverse. Solid lines are phase boundaries in reference, dotted lines in **b** and **c** are the clinopyroxene–ilmenite phase boundary of Kirfel and Neuhaus (1974) for comparison.

293 and 1373 K, but only with very large temperature steps. Ashida et al. (1985) measured the room-temperature compressibility, thermal expansion between 300 and 1000 K, and heat capacity of ilmenite-structured $MgGeO_3$ between 150 and 700 K. Tsuchiya and Tsuchiya (2007) used density functional theory to compute a thermal equation of state for ilmenite-structured $MgGeO_3$ but did not investigate the pyroxene phases.

In this study, we attempt to unify the differing phase diagram topographies presented by experiments and thermodynamics. We performed high-pressure and -temperature quenching experiments to directly constrain the phase diagram of the $MgGeO_3$ system, and we also measured the thermal expansion of the three phases at ambient pressure. Fitting the thermal expansion volumes with a Debye-Grüneisen zero-pressure equation of state enables us to estimate the heat capacity and Clapeyron slope of the phase relations to compare with the direct experimental constraints.

Methods

Sample synthesis and high-pressure phase relations

Samples of orthopyroxene-structured $MgGeO_3$ were synthesized from stoichiometric mixtures of MgO and GeO_2. The oxides were ground in an agate pestle and mortar under isopropanol and pressed into pellets. The pellets were sintered at 1373 K for 72 h in air. Pellets were then crushed and ground under isopropanol for 20 min to generate a fine powder and analyzed by X-ray powder diffraction to determine their purity. This sintering and analysis process was repeated, with minor additions of MgO or GeO_2 based on the phase fractions determined from the diffraction patterns, until pure orthopyroxene-structured $MgGeO_3$ was synthesized.

Phase relations of $MgGeO_3$ at pressures less than ~1.5 GPa were examined using a piston-cylinder cell (Boyd and England 1960) and above ~1.5 GPa with a Walker type multi-anvil apparatus (Walker et al. 1990) at University College London. Multiple samples ($MgGeO_3$ and pressure calibrants) were contained in capsules of double-wrapped 25 μm Inconel625 ($Ni_{61}Cr_{22}Mo_9Fe_5$) foil, 3 mm long and 2.5 mm diameter; the samples were separated by disks of Inconel625.

Piston-cylinder experiments used $BaCO_3$ pressure media with graphite furnaces (OD 7.7 mm, ID 6.2 mm), and the inner parts of the cell, surrounding the capsule, were made from MgO. The capsule was loaded centrally with respect to the length of the furnace. Temperature was monitored using a K-type thermocouple, which was 1 mm above the end of the sample capsule (2.5 mm above the center of the furnace). A 1 mm thick corundum plate was placed between the sample capsule and the end of the thermocouple to prevent sample deformation.

The multi-anvil assembly used an 18 mm octahedral cell compressed by anvils with 11 mm corner truncations. The furnace comprised a 14 mm long double wrap of 25 μm thick Inconel 625 foil, with a diameter of 4 mm, inside a zirconia sleeve with an outer diameter of 6.25 mm. The inner parts were made of MgO as a confining medium and were large enough to hold the 3 mm long by 2.5 mm in diameter capsule. Temperature was monitored at the end of the sample capsule using a D-type ($W_{97}Re_3$-$W_{75}Re_{25}$) thermocouple. Thermocouples were shielded from the furnace using thin-walled corundum tubes with 0.8 mm outer diameter. The effects of pressure on thermocouple-emf were assumed to be negligible. The multi-anvil cell was calibrated using SiO_2, Ni_2SiO_4, Fe_2SiO_4, and Mg_2GeO_4 phase relations, in the same experiments as the $MgGeO_3$ phase relations were determined. The pressure calibrations indicated a large decrease in pressure in the temperature range 870–1370 K. The average pressure depression was 1.9 GPa, relative to a Bi calibration curve measured at room temperature.

The conditions of the synthesis and phase-relations experiments, as well as the run products are listed in Table 1. The phases present in all recovered samples were identified by X-ray diffraction. The phase boundary positions were determined by the first occurrence of the high-pressure phase and pass thought the middle of the constraints.

The samples of the high-pressure clinopyroxene-structured and ilmenite-structured $MgGeO_3$ for thermal expansion measurements were synthesized from the orthopyroxene phase using the same 18/11 multi-anvil cell. The clinopyroxene-structured $MgGeO_3$ was synthesized at 2.5 GPa and 1173 K for 3 h and $MgGeO_3$ ilmenite phase was synthesized at 5 GPa and 1373 K for 3 h. Each sample synthesis was recovered, ground in an agate pestle and mortar under isopropanol before analysis by X-ray powder diffraction to confirm phase purity. Several syntheses were required to produce the amount of material required for the thermal expansion measurements.

Thermal expansion measurements by X-ray powder diffraction

Ideally, all three samples would be measured by X-ray diffraction simultaneously, removing the possibility of any inconsistencies between measurements. However, there is a significant degree of peak overlap between the orthopyroxene phase and the other phases due to the large number of diffraction peaks in the orthopyroxene phase (see Fig. 2). The orthopyroxene phase was therefore run on its own while the clinopyroxene and ilmenite phases were mixed together and measured at the same time. The samples used for the diffraction experiments were mixed with high-purity MgO (Aldrich 99.99%). The MgO was fired overnight at 1073 K in air before mixing. The purpose of the MgO was to provide good constraints to the specimen transparency and displacement in the subsequent refinements—constraints that are not well provided by low-symmetry materials.

Unit-cell volumes as a function of temperature were investigated by X-ray diffraction using the same method as previous studies (e.g., Hunt et al. 2017; Pamato et al. 2018). We used a PANalytical X'Pert Pro diffractometer, with Bragg-Brentano parafocusing reflection geometry. The cobalt X-ray source is monochromated, by a Ge (111) Johansson geometry focusing monochromator, to produce a Co$K\alpha_1$ incident beam, the wavelength of which is assumed to be 1.788996 Å (Hölzer et al. 1997). The X-ray tube was operated at 40 kV and 30 mA. Variable-width divergence and anti-scatter slits were used, together with a 10 mm wide incident-beam mask, so as to illuminate a 10 × 8.5 mm area of the sample. Both the incident and diffracted beams had 0.04 radian Soller slits to reduce the axial divergences. The X-ray detector was an "X'Celerator" position-sensitive detector with an angular range of $2\theta = \pm 1.061°$ and an effective fixed step size of 0.0167°. Data were collected over the 2θ range from 20 to 154.9°. Prior to the experiments reported here, the zero 2θ angle of the diffractometer was determined using an Si standard.

Diffraction data between 40 and 300 K were collected using an Oxford Cryo-

Table 1. Experimental conditions and outcomes used here to synthesize samples and constrain the phase diagram

Expt.	Type	Pressure	Temperature	Duration	Sample	
		(GPa)	(K)	(h)	Starting	Recovered
synthesis	furnace	1 bar	1373	72	oxides	Opx
synthesis	MA	2.5	1173	3	Opx	Cpx
synthesis	MA	5.0	1273	3	Opx	Ilm
GER001	MA	2.1	1273	2	Opx	Cpx
GER003	MA	3.6	1173	3	Opx	Cpx
GER004	MA	2.6	1273	1.33	Opx	Cpx
GER005	MA	3.3	1273	1.5	Opx	Cpx
GER006	MA	4.6	1273	1.5	Opx	Ilm
GER007	MA	1.3	1073	1.5	Opx	Cpx+Opx
GER008[b]	MA	2.0	823	3	Opx	Cpx
GER011[b]	MA	2.6	823	20	Opx	Cpx
GER012	MA	3.9	1273	3	Opx	Cpx
GER013[a]	MA	4.2	1273	3	Opx	Cpx
GER014	MA	3.1	1123	3	Opx	Cpx
GER015[b]	MA	3.0	823	3	Opx	Cpx
GER017	MA	3.6	1123	3	Opx	1:9 Cpx:Ilm
GER018[a]	MA	3.1	1073	1	Opx	9:1 Cpx:Ilm
GER019	MA	2.9	1073	3	Opx	Cpx
GER020[a]	MA	3.3	1123	1	Opx	Cpx
GER022	MA	6.1	1523	2	Opx	Ilm
GER024[a]	MA	5.6	1473	2.66	Opx	Ilm
GER025	MA	5.4	1493	3	Opx	Cpx
GER028	MA	2.5	973	3	Opx	Cpx+Ilm
GER029[a]	PC	0.6	973	24	Opx	Opx
GER031[a]	PC	0.9	973	24	Opx	Cpx
GER032	PC	0.9	1323	4.5	Opx	Cpx
GER033	PC	1.2	1323	3	Opx	Cpx
GER035[a]	PC	0.3	1323	17.5	Opx	Opx
GER037[a]	PC	0.6	1273	3	Opx	Cpx+Opx
GER042	MA	5.0	1273	3	Opx	Ilm
GER043	MA	5.0	1273	3	Opx	Ilm
GER044	MA-R	3.0	1123	3.5	Ilm	Ilm+Cpx
GER046	MA-R	3.9	1273	3.5	Ilm	Ilm+Cpx

Notes: PC = piston cylinder experiment; MA = multi-anvil; MA-R = multi-anvil reversal. Samples: Opx = orthopyroxene; Cpx = clinopyroxene; Ilm = ilmenite.
[a] Experiments used to calculate the phase boundary positions.
[b] Experiments inferred to be kinetically inhibited.

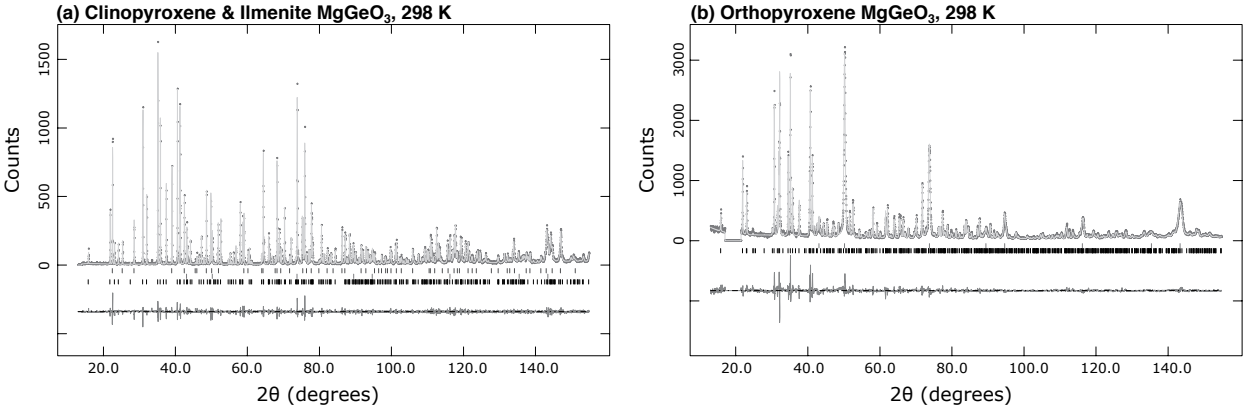

Figure 2. X-ray powder diffraction patterns showing the observations (points), calculated fit (upper line) and difference (lower trace) for (**a**) clinopyroxene and ilmenite $MgGeO_3$ and (**b**) orthopyroxene $MgGeO_3$ at 298 K. The tick marks show the positions of the Bragg reflections from (**a**) clinopyroxene, MgO, and ilmenite (top to bottom) and (**b**) MgO and orthopyroxene.

systems PheniX-FL low-temperature stage (Wood et al. 2018) and between 298 and 1173 K using an Anton Paar HTK1200N heating stage. The data were collected starting with the lowest temperature, in 20 K steps for the low-temperature stage and in 25 K steps for the high-temperature stage. In the PheniX-FL cold stage, the sample was held in an atmosphere of helium exchange gas. The temperature was cooled as quickly as possible (~3 K min^{-1}) to 80 K and then at 1 K min^{-1} to 40 K. After equilibration for 10 min at 40 K the data were collected. Subsequent increases in temperature were at 1 K min^{-1}, and the data were measured after ~15 min equilibration. The data collections were ~90 min long. In the high-temperature stage, the sample was heated at 5 K min^{-1}, after which it was equilibrated for 10 min and the data collected in a time of ~90 min.

Measurements in the high-temperature stage were made with the sample chamber open to the atmosphere. Data were collected in the orthopyroxene phase up to 1173 K. No additional diffraction peaks, produced by either back-transformation of the high-pressure phases to orthopyroxene-$MgGeO_3$ or by a reaction to form olivine-Mg_2GeO_4, were observed in any of the high-temperature measurements or in diffraction patterns taken from the samples after recovery to room temperature. The measurements of the clinopyroxene and ilmenite phases were stopped at 923 K when an additional diffraction peak appeared in the data.

The data were analyzed using the GSAS suite of programs (Larson and Von Dreele 2000; Toby 2001), after conversion from variable to fixed divergence slit geometry by the diffractometer manufacturer's X'pert HighScorePlus software package. The data was refined sequentially starting with the data collected closest to room temperature. The initial model for each refinement was the converged fit of the preceding temperature, except for the data closest to room temperature, which used the volumes and atomic coordinates from Yamanaka et al. (1985, 2005) as their starting point. Example diffraction patterns, from orthopyroxene and clinopyroxene + ilmenite, collected at 298 K are presented in Figure 2.

As has been previously found, the diffraction patterns of the clinopyroxene phase showed all the peaks consistent with the space group $C2/c$ and none of the additional peaks indicative of the $P2_1/c$ space group. The clinopyroxene (space group $C2/c$) and ilmenite (space group $R\bar{3}$) phases were analyzed using the Le Bail method (Le Bail et al. 1988). The Le Bail method produces less-biased cell parameters when fitting data from samples that might not be a true random powder pattern but at the cost of freely adjusting the intensity of each sample peak. In each refinement, the lattice parameters for the two $MgGeO_3$ phases (the triple-hexagonal cell was used for the ilmenite) and MgO (space group $Fm\bar{3}m$) were refined. Also refined were the peak profiles, specimen displacement and transparency, which were constrained to be the same for each sample in the diffraction pattern. At each temperature the fit achieved convergence with the data.

The larger unit cell and many overlapping low-intensity peaks in the orthopyroxene phase (space group *Pbca*) prevent the Le Bail method from producing well-constrained fits to the diffraction data. Therefore, the Rietveld method of refinement was used (Rietveld 1969). All the atoms in each phase (orthopyroxene-structured $MgGeO_3$ or MgO) were constrained to have the same isotropic thermal parameters (U_{iso}) and the two phases were constrained to have the same specimen transparency and displacement. Each pattern in the temperature series was initially fitted for the background coefficients and the unit cells of the MgO and orthopyroxene-structured $MgGeO_3$ phases, while the peak profile parameters, atomic positions, and thermal parameters of the orthopyroxene phase were fixed. When this refinement had converged these parameters were sequentially allowed to refine until all parameters were determined.

In the initial fits of the orthopyroxene phase data, there was a correlation between the unit-cell parameters and the poorly constrained sample transparency. Therefore, the data were re-fitted with a fixed sample transparency. For the low-temperature stage data, the mean of the consistent transparencies was used. For the high-temperature stage data, the free-fit transparencies decreased with temperature, slowly below 773 K and more quickly at higher temperatures. These values were smoothed using two first-degree polynomials that intersected at the change in slope in the transparency values. The data were subsequently re-refined using the transparency value of the polynomial at the relevant temperature.

In both 40 K diffraction patterns, reflections from β-nitrogen were observed. It was included in the refinement with space group $P6_3/mmc$. Following the unphysical model of Vegard (1932), the N_2 molecules were assumed to be spherical and the size compensated for by unusually large thermal vibrations.

There is a small offset (<2 in 10^4) in the lattice parameters and volumes between the high- and low-temperature diffraction stages. To compensate for this in the subsequent analysis the high-temperature data were multiplied by a scale factor to align them with the low-temperature data. The scaling was done by minimizing the residuals of a third-degree polynomial passing through the 10 data between 220–398 K. The scaling has minimal effect on the fitted thermophysical parameters; with and without scaling the data, they were all within two standard errors of each other and most parameters were within one standard error.

Results

Phase relations at high pressure and temperature

The pressure-temperature conditions at which we have synthesized the different phases of $MgGeO_3$ are presented in Figure 3a and Table 1. The phase boundaries constrained here are compared to those of other studies in Figure 3b. The experiments that constrain the position of the phase boundary are noted in Table 1. We find that below ~900 K the reaction kinetics are slow and the reaction does not run to completion even after 20 h. This is consistent with the inferred experimental constraints of Kirfel and Neuhaus (1974) who report no experiments below 923 K. Above ~900 K reaction kinetics are fast, running to completion within 1 h at 1123 K and 24 h at 973 K.

There is disagreement between studies as to which phase is the stable phase of $MgGeO_3$ between ~900 and 1273 K at ambient pressure (Fig. 1). Kirfel and Neuhaus (1974) find the orthopyroxene phase is stable in this temperature range (Fig. 1a), while Ross

and Navrotsky (1988) argue the clinopyroxene phase is the stable ambient pressure below 973 K (Fig. 1b). Ozima and Akimoto (1983) argue the orthopyroxene phase is stable between 1083 and 1173 K, transforming to the clinopyroxene or protopyroxene phase at lower and higher temperatures, respectively.

During our high-temperature X-ray diffraction measurements (up to 1173 K) we did not observe any sign of the orthopyroxene phase transforming to the clinopyroxene phase despite the sample being hotter than 900 K for over 34 h and hotter than 1023 K for 22 h by the end of the experiment. However, during the clinopyroxene and ilmenite phase X-ray diffraction measurements, a new diffraction peak appeared around 900 K; identification of which was prevented by termination of the measurement. No phase transformation is to be expected at temperatures <900 K based on the reaction kinetics inferred from the high-pressure experiments in this study. Therefore, the onset of reaction around 900 K in the clinopyroxene or ilmenite phase but not in the orthopyroxene phase indicates that the orthopyroxene phase is the stable phase at ~900 K and ambient pressure. Between 900 and 1173 K, the orthopyroxene phase remains the stable phase on the basis that there is no sign of transformation during the X-ray diffraction measurements. This is consistent with the observations of Yamanaka et al. (1985), who transformed the clinopyroxene phase to orthopyroxene at 1173 K in 1 h but the orthopyroxene phase showed no signs of transformation after 24 h at 973 K. The orthopyroxene phase is therefore shown to be the stable phase at ambient pressure at temperatures between 900 K and 1828 ± 5 K. We note that it is not possible to determine if the orthopyroxene phase ceases to be the stable phase below 900 K because of retarded reaction kinetics.

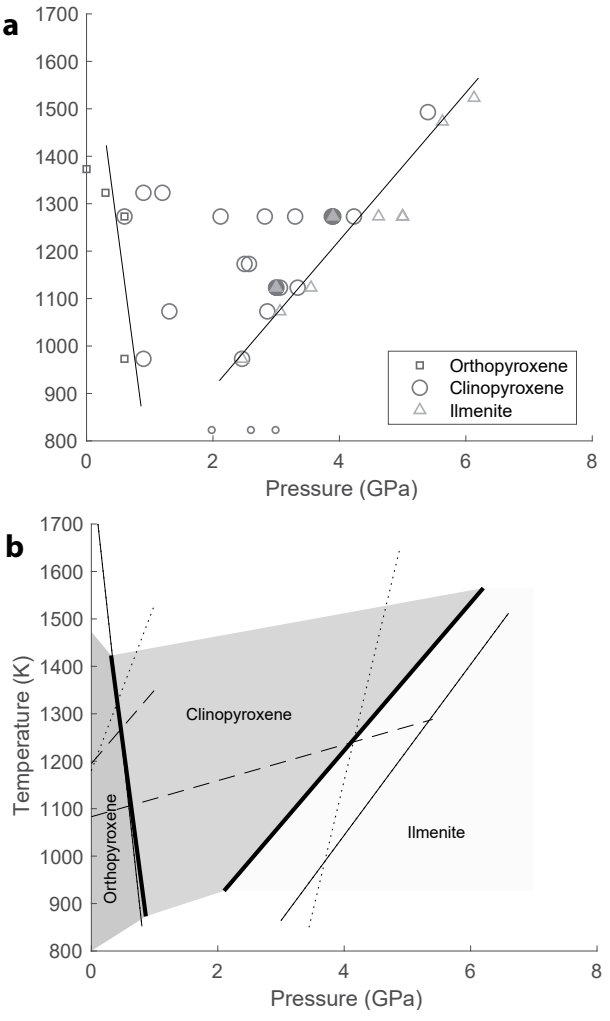

Figure 3. (**a**) $MgGeO_3$ phase diagram from the experiments in this study and (**b**) comparison of our phase boundaries (bold solid line) with those of Kirfel and Neuhaus (1974; solid line), Ozima and Akimoto (1983; dashed line) and Ross and Navrotsky (1988; dotted line). Symbols: square = orthopyroxene, circle = clinopyroxene, upward-pointing triangle = ilmenite, downward-pointing triangle = protopyroxene, open = forward, and filled = reversals. Small symbols denote experiments that were kinetically inhibited. Colored regions in **b** are the extent of the phase fields constrained by our experiments.

Our experimental phase diagram is consistent with most of the previous experimental data (Fig. 1) and like previous studies we find that ilmenite-structured $MgGeO_3$ is the high-pressure phase. The clinopyroxene-ilmenite phase boundary is constrained to have a Clapeyron slope of 6.4 +0.1/–0.6 MPa/K and to intercept 0 GPa at 600 K. This is in better agreement with the experimentally constrained 5.45 MPa/K of Kirfel and Neuhaus (1974) (Table 2) than the value of 1.9(4) MPa/K calculated by Ross and Navrotsky (1988) from calorimetry data. Our clinopyroxene-ilmenite phase boundary is ~1 GPa lower in pressure than that of Kirfel and Neuhaus (1974) (Figs. 1a and 3b), which could be due to differences in pressure calibration between the studies.

The orthopyroxene-clinopyroxene phase boundary occurs at <1 GPa, consistent with the experiments of Ringwood and Seabrook (1962) and Kirfel and Neuhaus (1974). Our experiments give a Clapeyron slope of –1.0 +1.0/–0.7 MPa/K, which intercepts 0 GPa at 1736 K. Given that the phase boundary is sub-parallel to the temperature axis, the value of 1736 K is very close to the 1 atm value of 1828 K determined by Robbins and Levin (1959). Our phase boundary is in excellent agreement with the study of Kirfel and Neuhaus (1974); who also found a negative but slightly shallower Clapeyron slope of –0.82 MPa/K but who fixed their

Table 2. Clapeyron slopes of the phase boundaries reported here and in previous studies

Author	Type	Clapeyron slope (MPa/K)	ΔS (J/K/mol)
Orthopyroxene-clinopyroxene			
This study	Experimental	$-1.0^{+1.0}_{-0.7}$	1.17[a]
Kirfel & Neuhaus (1974)	Experimental	–0.82	0.96[a]
Ozima & Akimoto (1983)	Experimental	28	–32.69[a]
Ross & Navrotsky (1988)	Calorimetry	2.1	–3
This study	Calculated (Debye, 1736 K)	16.0(0)[b]	–15.67(1)
This study	Calculated (αT, 1736 K)	–1.76(0)[b]	1.72(6)
Clinopyroxene-ilmenite			
This study	Experimental	$6.4^{+1.0}_{-0.6}$	–23.55[a]
Kirfel & Neuhaus (1974)	Experimental	5.45	–19.98[a]
Ross & Navrotsky (1988)	Calorimetry	2.0(4)	–7.6(15)
This study	Calculated (Debye, 600 K)	2.8(0)[b]	–10.34(7)
This study	Calculated (αT, 600 K)	3.1(0)[b]	–11.53(9)

Notes: The calculated Clapeyron slopes are reported at the temperature of the experimental phase boundary at 0 GPa; for the temperature evolution of the calculated Clapeyron slopes see Figure 9. The heat capacities used to calculate the Clapeyron slope were either the Debye heat capacity (Eq. 10) or the anharmonic heat capacity (αT, Eqs. 11 and 12); see text for details.

[a] ΔS values are calculated using the ΔV from the thermal expansion measurements in this study at 900 K.

[b] Errors are $<5 \times 10^{-4}$ but >0.

TABLE 3. Unit-cell parameters and volumes of $MgGeO_3$ phases measured in this study

Temperature	Orthopyroxene (*Pbca*)				Clinopyroxene (*C*2/*c*)				
(K)	Volume (Å^3)	*a* (Å)	*b* (Å)	*c* (Å)	Volume (Å^3)	*a* (Å)	*b* (Å)	*c* (Å)	β (°)
Low-temperature stage									
40	897.40(3)	18.7970(3)	8.9438(2)	5.33798(9)	433.156(8)	9.58991(8)	8.92315(7)	5.15484(4)	100.898(1)
60	897.25(2)	18.7966(3)	8.9432(2)	5.33753(9)	433.181(7)	9.59022(7)	8.92339(7)	5.15485(4)	100.899(1)
80	897.41(2)	18.7979(3)	8.9439(2)	5.33773(9)	433.197(8)	9.59042(8)	8.92348(7)	5.15491(4)	100.900(1)
100	897.48(2)	18.7979(3)	8.9443(2)	5.33786(9)	433.282(7)	9.59116(7)	8.92414(7)	5.15524(4)	100.906(1)
120	897.66(2)	18.7989(3)	8.9450(2)	5.33823(9)	433.335(7)	9.59174(8)	8.92467(7)	5.15532(4)	100.910(1)
140	897.83(2)	18.8003(3)	8.9457(2)	5.33847(9)	433.431(7)	9.59270(7)	8.92551(7)	5.15555(4)	100.915(1)
160	898.13(2)	18.8019(3)	8.9468(2)	5.33914(9)	433.530(7)	9.59370(7)	8.92637(7)	5.15582(4)	100.923(1)
180	898.40(2)	18.8035(3)	8.9481(2)	5.33951(9)	433.666(7)	9.59490(7)	8.92760(7)	5.15621(4)	100.930(1)
200	898.73(2)	18.8044(3)	8.9496(2)	5.34033(9)	433.797(7)	9.59599(7)	8.92891(7)	5.15656(4)	100.937(1)
220	898.95(2)	18.8057(3)	8.9507(1)	5.34053(9)	433.976(7)	9.59770(7)	8.93027(7)	5.15710(4)	100.945(1)
240	899.47(2)	18.8086(3)	8.9527(2)	5.34170(9)	434.147(8)	9.59893(8)	8.93187(8)	5.15767(5)	100.952(1)
260	899.78(2)	18.8108(3)	8.9536(2)	5.34235(9)	434.311(8)	9.60044(8)	8.93330(8)	5.15815(4)	100.962(1)
280	900.19(2)	18.8132(3)	8.9554(2)	5.34301(9)	434.499(8)	9.60203(8)	8.93500(8)	5.15868(4)	100.969(1)
300	900.62(2)	18.8153(3)	8.9571(2)	5.34392(9)	434.695(4)	9.60374(4)	8.93675(4)	5.15925(3)	100.978(0)[a]
High-temperature stage									
298	900.48(2)	18.8149(2)	8.9570(1)	5.34329(7)	434.755(6)	9.60388(6)	8.93706(6)	5.15955(4)	100.969(0)[a]
323	901.04(2)	18.8177(2)	8.9594(1)	5.34438(7)	435.015(9)	9.60617(8)	8.93911(8)	5.16041(5)	100.981(1)
348	901.59(2)	18.8214(2)	8.9614(1)	5.34542(7)	435.282(9)	9.60845(9)	8.94149(8)	5.16118(5)	100.992(1)
373	902.16(2)	18.8245(2)	8.9638(1)	5.34649(7)	435.598(9)	9.61106(9)	8.94406(8)	5.16226(5)	101.004(1)
398	902.75(2)	18.8278(2)	8.9662(1)	5.34755(7)	435.884(9)	9.61345(9)	8.94663(8)	5.16309(5)	101.016(1)
423	903.37(2)	18.8315(2)	8.9686(1)	5.34876(7)	436.194(9)	9.61621(9)	8.94916(8)	5.16407(5)	101.030(1)
448	903.96(2)	18.8348(2)	8.9710(1)	5.34995(7)	436.515(9)	9.61881(9)	8.95191(9)	5.16511(5)	101.043(1)
473	904.57(2)	18.8384(2)	8.9734(1)	5.35108(7)	436.840(10)	9.62149(9)	8.95476(9)	5.16610(5)	101.056(1)
498	905.20(2)	18.8419(2)	8.9759(1)	5.35232(7)	437.132(9)	9.62386(9)	8.95735(9)	5.16703(5)	101.070(1)
523	905.86(2)	18.8460(2)	8.9784(1)	5.35356(7)	437.466(10)	9.62665(9)	8.96023(9)	5.16806(5)	101.084(1)
548	906.48(2)	18.8499(2)	8.9808(1)	5.35471(7)	437.777(10)	9.62943(9)	8.96295(9)	5.16897(6)	101.101(1)
573	907.12(2)	18.8532(2)	8.9835(1)	5.35594(7)	438.135(11)	9.63240(9)	8.96581(10)	5.17021(6)	101.115(1)
598	907.75(2)	18.8570(2)	8.9857(1)	5.35723(7)	438.472(11)	9.63516(10)	8.96886(10)	5.17117(6)	101.129(1)
623	908.40(2)	18.8599(2)	8.9880(1)	5.35887(7)	438.848(11)	9.63833(10)	8.97200(10)	5.17240(6)	101.145(1)
648	909.05(2)	18.8638(2)	8.9904(1)	5.36015(7)	439.184(12)	9.64100(10)	8.97497(10)	5.17345(6)	101.158(1)
673	909.72(2)	18.8683(2)	8.9933(1)	5.36113(7)	439.530(12)	9.64394(11)	8.97798(11)	5.17452(6)	101.176(1)
698	910.42(2)	18.8722(2)	8.9961(1)	5.36246(7)	439.902(13)	9.64707(11)	8.98113(11)	5.17565(6)	101.190(1)
723	911.11(2)	18.8763(2)	8.9988(1)	5.36380(7)	440.257(13)	9.65001(12)	8.98412(11)	5.17680(7)	101.205(1)
748	911.80(2)	18.8796(2)	9.0012(1)	5.36546(7)	440.646(13)	9.65328(12)	8.98734(11)	5.17809(6)	101.223(1)
773	912.48(2)	18.8841(2)	9.0040(1)	5.36647(7)	441.048(14)	9.65617(12)	8.99095(12)	5.17944(7)	101.238(1)
798	913.16(2)	18.8879(2)	9.0067(1)	5.36781(7)	441.387(14)	9.65935(12)	8.99404(12)	5.18025(7)	101.255(1)
823	913.86(2)	18.8920(2)	9.0095(1)	5.36913(7)	441.769(15)	9.66238(13)	8.99703(13)	5.18166(7)	101.271(1)
848	914.59(2)	18.8956(2)	9.0120(1)	5.37090(7)	442.171(15)	9.66570(13)	9.00061(12)	5.18287(7)	101.289(1)
873	915.34(2)	18.9008(2)	9.0151(1)	5.37193(7)	442.564(15)	9.66900(13)	9.00383(13)	5.18416(7)	101.307(1)
898	916.08(2)	18.9049(2)	9.0180(1)	5.37339(7)	442.924(15)	9.67185(13)	9.00704(13)	5.18529(8)	101.322(1)
923	916.79(2)	18.9091(2)	9.0207(1)	5.37473(7)	443.323(16)	9.67517(14)	9.01032(13)	5.18661(8)	101.340(1)
948	917.55(2)	18.9135(2)	9.0237(1)	5.37619(7)					
973	918.29(2)	18.9175(2)	9.0267(1)	5.37755(7)					
998	919.04(2)	18.9221(2)	9.0294(1)	5.37905(7)					
1023	919.78(2)	18.9262(2)	9.0323(1)	5.38053(7)					
1048	920.58(2)	18.9310(2)	9.0353(1)	5.38205(7)					
1073	921.31(2)	18.9350(2)	9.0381(1)	5.38347(7)					
1098	922.12(2)	18.9397(3)	9.0414(1)	5.38491(8)					
1123	922.90(2)	18.9441(3)	9.0445(1)	5.38636(8)					
1148	923.67(2)	18.9476(2)	9.0473(1)	5.38826(7)					
1173	924.48(2)	18.9518(2)	9.0506(1)	5.38978(7)					
Scale factor									
	1.000087	1.000016	0.999979	1.000091	0.999821	0.999968	0.999948	0.999930	1.000079

Notes: The numbers in parentheses are one standard error of the least significant digit. Note, however, that the lattice parameter values listed here are probably less accurate than might be expected from the stated uncertainties, which are those reported from the Le Bail and Rietveld fits using GSAS; for further discussion of the importance of systematic errors in profile refinement of X-ray powder data see, e.g., Thompson and Wood (1983). Multiplying the high-temperature data by the scale factors aligns it with the low-temperature data; see text for details.

[a] Errors are $<5 \times 10^{-4}$ degrees but greater than zero.

(Table extends to next page)

0 GPa intercept to be 1828 K (Table 2; Figs. 1 and 3). Our phase boundary would be in even better agreement with Kirfel and Neuhaus (1974) if we also fixed the 0 GPa intercept to 1828 K. These results contradict the studies of Ozima and Akimoto (1983) and Ross and Navrotsky (1988) who both argued for a positive Clapeyron slope.

Ozima and Akimoto (1983) report simultaneously flux growing orthopyroxene, clinopyroxene, and "clinopyroxene from protopyroxene" phases in the temperature range 928–1228 K. Yamanaka et al. (1985) quenched the orthopyroxene phase from a flux at 1823 K and recovered the clinopyroxene phase by slow cooling from a flux at 1633 K. Both studies argue for *C*2/*c* clinopyroxene as the low-temperature phase and neither report observing a $P2_1/c$ low-clinoenstatite phase. Ozima and Akimoto (1983) argue for the protoenstatite phase being stable above 1173 K based on the recovery of two different styles of clinopyroxene phase from their flux. The incompatibility of these studies with our and other studies is possibly due to flux contamination compared to direct growth from oxides.

The phase boundaries in our experiments converge toward lower pressure and temperature, and in the absence of other phases, the triple point is at 0.98 GPa and 752 K. This is in good agreement

TABLE 3.—*EXTENDED*

Temperature	Ilmenite ($R\bar{3}$)		
(K)	Volume (Å^3)	*a* (Å)	*c* (Å)
	Low-temperature stage		
40	289.134(5)	4.93239(5)	13.72313(15)
60	289.150(5)	4.93246(4)	13.72352(14)
80	289.151(5)	4.93242(4)	13.72378(14)
100	289.198(5)	4.93270(4)	13.72448(14)
120	289.231(5)	4.93290(4)	13.72495(14)
140	289.281(5)	4.93313(4)	13.72598(14)
160	289.331(5)	4.93334(4)	13.72722(14)
180	289.415(5)	4.93376(4)	13.72887(14)
200	289.482(5)	4.93408(4)	13.73025(14)
220	289.592(5)	4.93464(4)	13.73233(14)
240	289.687(5)	4.93512(4)	13.73415(15)
260	289.795(5)	4.93567(4)	13.73625(16)
280	289.896(5)	4.93614(4)	13.73841(15)
300	290.013(3)	4.93671(2)	13.74081(9)
	High-temperature stage		
298	290.057(4)	4.93703(3)	13.74110(12)
323	290.218(6)	4.93801(5)	13.74328(16)
348	290.374(6)	4.93869(5)	13.74681(16)
373	290.568(6)	4.93970(5)	13.75043(15)
398	290.745(6)	4.94063(5)	13.75363(15)
423	290.939(6)	4.94162(5)	13.75729(15)
448	291.130(6)	4.94261(5)	13.76080(16)
473	291.336(6)	4.94365(5)	13.76475(16)
498	291.511(6)	4.94447(5)	13.76841(15)
523	291.706(6)	4.94545(5)	13.77223(15)
548	291.899(6)	4.94646(5)	13.77566(16)
573	292.125(6)	4.94772(5)	13.77933(16)
598	292.340(7)	4.94883(5)	13.78326(17)
623	292.561(7)	4.94993(6)	13.78760(17)
648	292.767(7)	4.95101(6)	13.79129(17)
673	292.975(8)	4.95208(6)	13.79509(18)
698	293.210(8)	4.95328(6)	13.79945(19)
723	293.420(8)	4.95435(6)	13.80343(18)
748	293.671(8)	4.95564(6)	13.80803(18)
773	293.930(8)	4.95696(6)	13.81284(19)
798	294.126(8)	4.95800(6)	13.81619(19)
823	294.373(8)	4.95923(6)	13.82100(20)
848	294.617(8)	4.96050(6)	13.82538(20)
873	294.863(9)	4.96178(6)	13.82971(20)
898	295.088(9)	4.96291(7)	13.83406(21)
923	295.309(9)	4.96404(7)	13.83804(21)
948			
973			
998			
1023			
1048			
1073			
1098			
1123			
1148			
1173			
	Scale factor		
	0.999807	0.999914	0.999978

with the triple point position of Kirfel and Neuhaus (1974) that is at 1.07 GPa and 517 K.

Thermal expansion

The unit-cell volumes of the $MgGeO_3$ orthopyroxene, clinopyroxene, and ilmenite phases are listed in Table 3 and plotted, as normalized values, in Figures 4, 5, and 6, respectively. The unit-cell parameters measured here at 298 and 300 K show a good correspondence to previously reported values at ambient conditions (Table 4) and have significantly lower standard errors. Our values for clino- and orthopyroxene phases are within the range of previous values. For the ilmenite phase, our more precise values correspond reasonably to those of previous studies; our measured unit-cell volume and *c*-axis agree within 2 standard errors and the *a*-axis agrees to 5 standard errors of the values of Ashida et al. (1985).

Only two other studies have reported high-temperature unit-cell parameters for the $MgGeO_3$ phases studied here: Yamanaka et al. (1985) and Ashida et al. (1985). Yamanaka et al. (1985) report the unit-cell parameters of clinopyroxene-structured $MgGeO_3$ at five temperatures between 298 and 1023 K and at 298, 1223, and 1373 K for the orthopyroxene-structured $MgGeO_3$. Their unit-cell parameters are always larger than those reported here (Figs. 4 and 5) and the difference between their data and ours increases with temperature. Conversely, the unit-cell volumes from Ashida et al. (1985) are always smaller than those measured here; again, the difference increases with temperature. The increasing differences in unit-cell parameter with temperature might imply that the differences come from inaccuracies in thermometry. We have calibrated our experi-

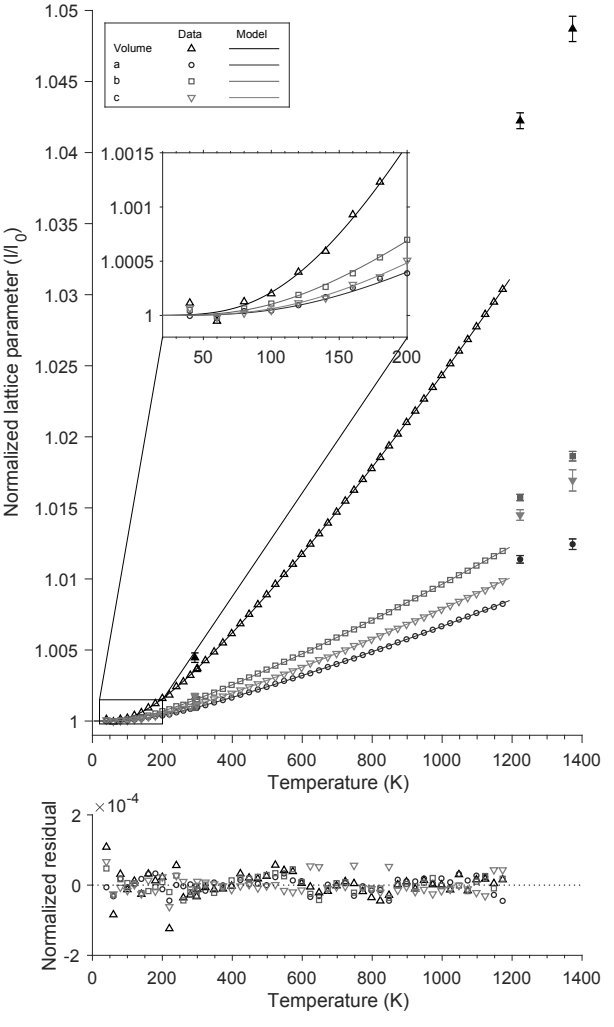

FIGURE 4. (**top**) Lattice parameters, unit-cell volumes and (bottom) residuals to fit of orthopyroxene $MgGeO_3$ (Table 3), normalized to the 0 K values reported in Table 5. The error bars are omitted for clarity and the high-temperature measurements are multiplied by the scale factor. Lines are normalized fits of the Debye-Grüneisen model to the data of this study. Filled symbols are the data from Yamanaka et al. (1985).

mental apparatus using the melting point of gold (Pamato et al. 2018) and the thermal expansivity of silicon (Lindsay-Scott et al. 2007) and find excellent agreement with literature data for these two calibration methods. We therefore believe the present thermometry and unit-cell parameter measurements to be the most accurate of the three studies. If the differences between the present data and the previous studies are due to inaccuracies in thermometry it would require temperature errors in excess of 10% in the previous studies.

The Le Bail method does not give the atomic positions of the atoms within the unit cell but the Rietveld refinement used for the orthopyroxene phase gives atomic positions which, while poorly constrained, are overall consistent with those of Yamanaka et al. (1985).

Volume-temperature models. For many materials, at elevated temperatures (>298 K), the change in unit-cell volume and axes with temperature is well approximated by the integral over a low-degree polynomial. This empirical form of thermal expansion has the formulation (Fei 1995):

$$l(T) = l_{T_{\mathrm{ref}}} \exp\left[\int_{T_{\mathrm{ref}}}^{T} \alpha(T)\,\mathrm{d}T\right] \quad (1)$$

where $l_{T\mathrm{ref}}$ is a unit-cell parameter (i.e., V, a, b, c) at a reference temperature, T_{ref}, and $\alpha(T)$ is the thermal expansivity, the second-degree form of which is

$$\alpha(T) = a_0 + a_1 T + a_2 T^{-2}. \quad (2)$$

Here, the reference temperature is taken as 298 K and values of $l_{T_{\mathrm{ref}}}$, a_0, a_1, and a_2 for the unscaled high-temperature stage data in this study are listed in Table 5. Also listed are the equivalent parameters for the experimental data of Yamanaka et al. (1985) and Ashida et al. (1985) as well as calculations of Tsuchiya and Tsuchiya (2007). The data density of this study enabled utilization of the second-degree form of the thermal expansivity but the sparser data of the other studies mean it is only reasonable to report the zeroth- or first-degree forms.

For the clinopyroxene phase, except for the β angle, the values of a_0 derived from the study of Yamanaka et al. (1985) are more than one standard error greater than those in this study, which is not unexpected given their larger unit-cell parameters. Only the volumetric thermal expansivity of the ilmenite-structured phase is calculable from the data of Ashida et al. (1985) and this is within error of our value at the reference temperature (298 K) but does not increase at the same rate as that of this study. Again, this might be expected because of the smaller volumes measured in that study.

In the orthopyroxene phase, the axial thermal expansions occur in the same order as those of Yamanaka et al. (1985), $\alpha_b > \alpha_c > \alpha_b$, but with slightly different values. In the clinopyroxene phase both studies agree that $\alpha_b > \alpha_a > \alpha_c$. The order of these axial thermal expansions is the same as those in the equivalent polymorphs in $MgSiO_3$ (Hugh-Jones 1997).

For the ilmenite phase, the calculated thermal expansion of Tsuchiya and Tsuchiya (2007) is less than that measured here.

At low temperatures, the thermal expansion does not follow a simple low-order polynomial form. Instead, the Debye model can be used to provide a theoretical description of the internal energy (U) that, when combined with further theory, leads to a representation of the thermal expansion that has the observed low-temperature functional form. The internal energy predicted by the Debye model is (e.g., Poirier 2000):

$$U(T) = 9Nk_{\mathrm{B}}T\left(\frac{T}{\theta_{\mathrm{D}}}\right)^3 \int_0^{\theta_{\mathrm{D}}/T} \frac{x^3}{\exp(x)-1}\,\mathrm{d}x \quad (3)$$

where N is the number of atoms in the unit cell, k_B is Boltzmann constant, and θ_D is the Debye temperature. The purely harmonic oscillators in this model do not predict thermal expansion and, therefore, this model has been combined with the Grüneisen approximations to form a zero pressure, quasi-harmonic, equation of state (Wallace 1998), in which the effects of thermal expansion are considered equivalent to elastic strain, induced by thermal pressure. Further expansions to the internal energy model that account for intrinsic anharmonicity (Oganov and Dorogokupets 2004) have also been developed. Previous studies (e.g., Vočadlo et al. 2002; Lindsay-Scott et al. 2007) have shown that a second-order Grüneisen approximation, combined with quasi-harmonic Debye internal energy model, provides a satisfactory description of data covering a wide range of temperatures, albeit sometimes additional modifications are required (e.g., Hunt et al. 2017; Pamato et al. 2018). It has the form (Wallace 1998):

$$V(T) = V_0 + \frac{V_0 U}{Q - bU} \quad (4)$$

where

$$Q = V_0 K_0/\gamma \quad (5)$$

and

$$b = (K' - 1)/2 \quad (6)$$

$V(T)$ is the unit-cell volume at finite temperature, V_0 is its 0 K value, K_0 and K' are the bulk modulus and its first pressure derivative, and γ is a Grüneisen parameter, which in the derivation is assumed to be constant. In assuming that γ is independent of temperature, it becomes equivalent to the thermodynamic Grüneisen parameter, γ_{th} (Wallace 1998); for a full explanation the reader is referred to Poirier (2000) and Wallace (1998). Expressions of the same functional form as Equation 4 may also be used to describe the behavior of the axes of the crystal but with a different interpretation of the values of the parameters Q and b (Lindsay-Scott et al. 2007).

Equation 4 was fitted to the unit-cell parameter—temperature data by minimizing the sum of the weighted least-squared residuals; the axial values were fitted as measured, rather than pseudo-cubic values. The standard errors of the measurements were used to calculate the weights. Unlike in our previous studies (Hunt et al. 2017; Pamato et al. 2018) the 40 K data point was not additionally weighted because of greater scatter in the low-temperature unit-cell parameters of the orthopyroxene phase. The additional scatter is possibly due to the increased number peaks in the orthopyroxene unit cell and the larger numbers of free parameters in the GSAS fitting. We expect this scatter to have only a minor effect on the subsequent analysis.

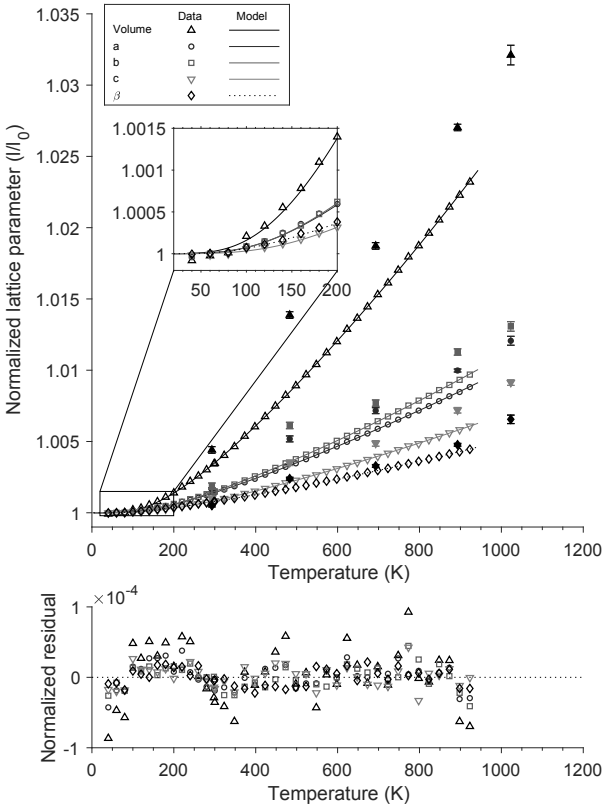

Figure 5. (**top**) Lattice parameters, unit-cell volumes, and (**bottom**) residuals to fit of clinopyroxene $MgGeO_3$ (Table 3), normalized to the 0 K values reported in Table 5. The error bars are omitted for clarity and the high-temperature measurements are multiplied by the scale factor. Lines are normalized fits of the Debye-Grüneisen model to the data of this study. Filled symbols are the data from Yamanaka et al. (1985).

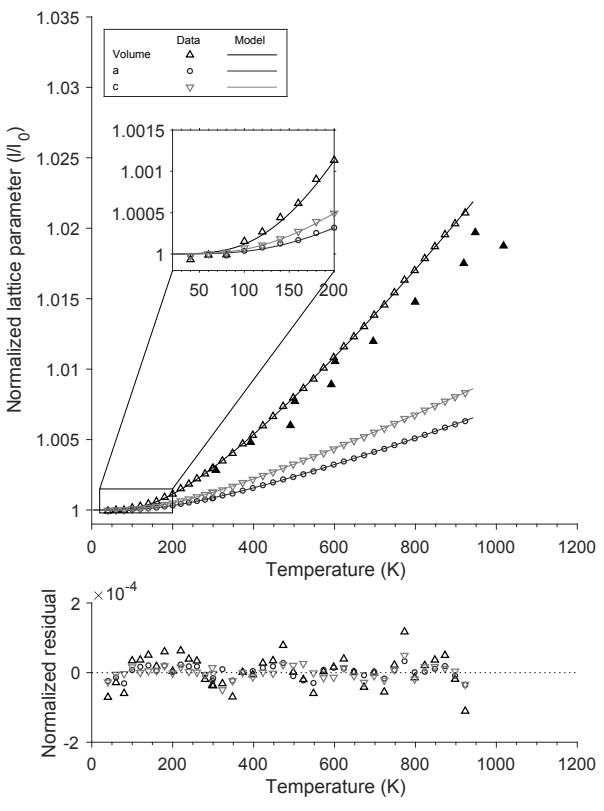

Figure 6. (**top**) Lattice parameters, unit-cell volumes, and (**bottom**) residuals to fit of ilmenite $MgGeO_3$ (Table 3), normalized to the 0 K values reported in Table 5. The error bars are omitted for clarity and the high-temperature measurements are multiplied by the scale factor. Lines are normalized fits of the Debye-Grüneisen model to the data of this study. Filled symbols are the data from Ashida et al. (1985).

Table 4. Unit-cell parameters from previous studies at ambient conditions

	Reported temperature	V (Å^3)	a (Å)	b (Å)	c (Å)	β (°)
		Orthopyroxene				
This study	298 K	900.48(2)	18.8149(2)	8.9570(1)	5.34329(7)	
	300 K	900.62(2)	18.8153(3)	8.9571(2)	5.34392(9)	
Roth (1955, 1957)	–	–	18.661	8.954	5.346	
Lyon (1968)	–	–	18.745(5)	8.974(17)	5.350(1)	
Lindemann (1961)	–	–	18.649(7)	8.902(5)	5.332(5)	
Kirfel and Neuhaus (1974)	–	901.17(35)	18.859(6)	8.958(2)	5.334(1)	
Ozima (1983); Ozima and Akimoto (1983)	–	899.69	18.8099(12)	8.9484(8)	5.3451(4)	
Yamanaka et al. (1985)	20 °C	901.3(3)	18.829(3)	8.952(2)	5.347(1)	
		Clinopyroxene				
This study	298 K	434.755(6)	9.60388(6)	8.93706(6)	5.15955(4)	100.969(0)[c]
	300 K	434.695(4)	9.60374(4)	8.93675(4)	5.15925(3)	100.978(0)[c]
Kirfel and Neuhaus (1974)	–	440.0(5)	9.623(9)[a]	8.960(5)	5.196(3)	100.144(8)
Ozima (1983); Ozima and Akimoto (1983)	–	434.27(6)	9.6010(8)	8.9323(6)	5.1592(5)	101.034(9)
Yamanaka et al. (1985)	20 °C	435.1(1)	9.605(2)	8.940(2)	5.160(1)	100.95(1)
		Ilmenite				
This study	298 K	290.057(4)	4.93703(3)		13.74110(12)	
	300 K	290.013(3)	4.93671(2)		13.74081(9)	
Ringwood and Seabrook (1962)	–	–	4.936(5)		13.76(5)	
Kirfel and Neuhaus (1974)	–	289.8	4.936(1)		13.735(5)	
Kirfel et al. (1978)	–	289.80(14)	4.933(1)		13.734(5)	
Ito and Matsui (1979)	"ambient conditions"	–	4.9363(2)		13.7401(8)	
Ashida et al. (1985)	273 K	289.93	–		–	
Tsuchiya and Tsuchiya (2007)	300 K	291.48[b]	4.949[b]		13.743[b]	

Notes: Values not reported are marked "–", numbers in parentheses are the standard error in the last digit and numbers without parentheses did not have reported errors. All unit-cell parameters were measured by powder or single-crystal X-ray diffraction unless otherwise noted. See note in caption of Table 3 regarding significance of values determined in this study. [a] Value was reported as twice this value. [b] Calculated using density functional theory. [c] Error is $<5 \times 10^{-4}$ degrees but >0.

TABLE 5. Polynomial thermal expansion parameters derived from the high-temperature data in Table 3, together with selected other data

	$l_{298\ K}$	a_0 (×10^{-6} K^{-1})	a_1 (×10^{-9} K^{-2})	a_2 (K)
		This study—Orthopyroxene		
V	900.47402 Å^3	23.46(4)	9.65(7)	−0.169
a	18.81493(19) Å	7.01(9)	2.22(12)	−0.107
b	8.95700(7) Å	8.45(7)	4.52(9)	0.034
c	5.34326(6) Å	7.99(10)	2.92(14)	−0.096
		This study—Clinopyroxene		
V	434.75207 Å^3	25.79(15)	11.73(29)	−0.456
a	9.60388(5) Å	9.89(9)	4.15(16)	−0.157
b	8.93700(5) Å	11.53(9)	4.19(16)	−0.270
c	5.15954(3) Å	6.01(11)	4.28(18)	−0.068
β	100.96923°	4.95(4)	2.22(7)	−0.120
		This study—Ilmenite		
V	290.05569 Å^3	23.32(20)	11.66(39)	−0.429
a	4.93707(4) Å	6.84(13)	3.89(21)	−0.122
c	13.74079(14) Å	9.58(16)	3.93(27)	−0.179
		Yamanaka et al. (1985)—Orthopyroxene		
V	901.476(64) Å^3	39.8(1)		
a	18.830(3) Å	10.1(3)		
b	8.953(2) Å	15.9(3)		
c	5.347 Å	13.7(2)		
		Yamanaka et al. (1985)—Clinopyroxene		
V	435.433 Å^3	43.8(132)	−13.4(233)	
a	9.608(5) Å	16.7(67)	−5.1(104)	
b	8.944(7) Å	18.4(100)	−5.9(155)	
c	5.161(2) Å	7.7(54)	4.4(80)	
β	100.968(36)°	7.9(52)	−1.6(84)	
		Ashida et al. (1985)—Ilmenite		
V	289.816 Å^3	25.7(44)	−2.3(74)	
		Tsuchiya and Tsuchiya (2007)—Ilmenite		
V	291.48 Å^3 [a]	20.9[a]		

Notes: Numbers in parentheses are the standard error in the least significant digit; numbers without errors have a standard error of <0.5 least significant digit.
[a] 0 GPa, 300 K values calculated using density functional theory.

There is a suggestion of negative thermal expansion in orthopyroxene phase at the lowest temperatures, both in the axial and volumetric values. The 40 K data, where the negative thermal expansion may be observed, is also where we observe β-N_2 in the diffraction pattern. The data density and 40 K temperature limit of the PheniX-FL stage preclude fitting the data with multiple Debye or Einstein internal energy modes. We note that negative thermal expansion is observed at low temperatures in the germanate pyroxenes $CoGeO_3$ (Redhammer et al. 2010a) and $P2_1/c$ $LiFeGe_2O_6$ (Redhammer et al. 2010b) but not in the silicate jadeite (Knight and Price 2008).

Table 6 lists the thermophysical parameters returned by the fit and the values derived from these. The fits are plotted in Figures 4, 5, and 6 as lines. The model provides a good fit to the data, except at perhaps the very lowest temperatures in the orthopyroxene phase. The residuals are slightly systematic with temperature, but higher and lower order Grüneisen approximations result in worse fits. There is not sufficient temperature range in the data to adequately constrain anharmonic internal energy models (Oganov and Dorogokupets 2004).

For each phase, the volumetric Debye temperature is bracketed by the axial Debye temperatures and, for each phase, the a_0 values (Eq. 2; Table 5) are proportional to $1/Q$ (Table 6). The Debye temperatures reported from heat capacity by Ashida et al. (1985) for ilmenite phase (Table 6) are larger than we calculate here, whereas the Debye temperatures calculated for clinopyroxene and ilmenite phases from the sound velocity data of Liebermann (1974) are slightly smaller. The acoustic Debye temperature has been found to be up to ~80 K lower than the thermal Debye temperature in pyroxene structured phases (Yang and Ghose 1994) and it would appear that same is true for ilmenite-structured phases.

The values of *b* imply volumetric K' values (Table 6) significantly greater than the 3.6 measured in ilmenite-structured $MgGeO_3$ (Ashida et al. 1985) and the 4.59 calculated for ilmenite-structured $MgGeO_3$ (Tsuchiya and Tsuchiya 2007). They are also greater than the values of K' typically reported for oxides and silicate minerals ($3 < K' < 8$, Knittle 1995). The values of K' in $MgSiO_3$ pyroxenes have been measured to be greater than 5.6(29) (Angel and Hugh-Jones 1994; Angel and Jackson 2002), but no values exist for $MgGeO_3$ pyroxene-structured phases.

The Grüneisen parameter (γ, Eq. 5) is derived using the bulk modulus. The bulk modulus of ilmenite-structured $MgGeO_3$ has been measured to be 187(2) GPa (Sato et al. 1977), 195 GPa (Ashida et al. 1985), and 180(2) GPa (Yamanaka et al. 1985). The bulk modulus of orthopyroxene-structured $MgGeO_3$ is 115 GPa (Ross and Navrotsky 1988) and Liebermann (1974) measured K_s = 131 GPa at 0.75 GPa pressure in the clinopyroxene phase. The adiabatic bulk modulus (K_S) is related to the isothermal bulk modulus (K_T) by:

$$K_S = K_T (1 + \gamma_{th} \alpha T) \quad (7)$$

Assuming that K_T is isothermal and equal to K_0 and that γ_{th}, the thermodynamic Grüneisen parameter is equal to γ (Eq. 5; Wallace 1998), it is possible to solve for γ using a value of K_S.

Using the values above and for the clinopyroxene phase Equation 7, we calculate γ to be 0.86, 1.01 (at 300 K), and 1.23 for the orthopyroxene, clinopyroxene, and ilmenite phases, respectively (Table 6). The effect of converting K_S to K_T for the clinopyroxene phase is minimal; calculating γ directly using K_S yields a value of 1.02(1). For ilmenite, Tsuchiya and Tsuchiya (2007) used density functional theory to calculate a value for γ of 1.24, which is very close to our value.

The thermal expansivity (α) is the derivative of the unit-cell parameter with respect to temperature:

$$\alpha(T) = \frac{1}{l(T)}\left(\frac{dl}{dT}\right) \quad (8)$$

where *l* is the unit-cell length (for axial expansivities) or volume (for volumetric expansivities). The point-to-point volumetric thermal expansivity of the $MgGeO_3$ phases is plotted in Figure 7, together with the thermal expansion calculated from the polynomial and Debye-Grüneisen models. At low temperatures, the orthopyroxene phase has a greater thermal expansion than the clinopyroxene or the ilmenite phases, which is reflected in the lower Debye temperature in this phase (Table 6). Consistent with the polynomial thermal expansion coefficients and the *b*-values of the Debye model, at elevated temperatures, the thermal expansivity of the orthopyroxene phase increases with temperature significantly slower than that of the other two phases.

Heat capacity

The Debye model of internal energy also can be used to calculate a heat capacity. The isochoric or volumetric heat capacity is the change in internal energy (*U*), at constant volume, with temperature:

Table 6. Debye-Grüneisen model thermophysical parameters and derived values

		l_0	θ_D (K)	Q (×10^{-16} J)	*b*	*K'*	γ
This study, thermal expansion							
Orthopyroxene	*V*	897.299(16) Å^3	602(7)	1.199(6)	4.6(1)	10.3(3)	0.861(5)[a]
	a	18.79709(21) Å	650(16)	4.22(5)	14(1)		
	b	8.94334(11) Å	545(11)	3.11(3)	12(1)		
	c	5.33762(7) Å	635(16)	3.61(5)	13(1)		
Clinopyroxene	*V*	433.192(7) Å^3	693(10)	0.56(1)	5.9(4)	12.7(9)	1.01(1)[b]
	a	9.59029(8) Å	633(12)	1.50(2)	15(1)		
	b	8.92336(6) Å	663(9)	1.36(1	15(1)		
	c	5.15493(3) Å	772(15)	2.03(3)	20(2)		
	β	100.8987(7)°	473(15)	3.47(5)	53(3)		
Ilmenite	*V*	289.154(5) Å^3	758(13)	0.44(1)	5.9(5)	12.7(11)	1.23(2)[c]
	a	4.93251(4) Å	801(18)	1.43(3)	18(2)		
	c	13.72349(10) Å	707(12)	1.13(1)	13(1)		
This study, from experimental Clapeyron slopes							
Clinopyroxene	Orthopyroxene-Clinopyroxene transition						1.07(4)
	Clinopyroxene-Ilmenite transition						1.08(3)
Ashida et al. (1985)							
Ilmenite	*V*		819 (all data) 777 (<300 K)			3.6	
Liebermann (1974)							
Clinopyroxene	*V*		618				
Ilmenite	*V*		657[d]				
Tsuchiya and Tsuchiya (2007)							
Ilmenite	*V*	291.48 Å^3[e]				4.59[e]	1.24[e]

[a] Calculated using K_T = 115 GPa.
[b] Calculated assuming K_S = 131 GPa.
[c] Calculated using K_T = 187 GPa.
[d] Reported in Okada et al. (2008).
[e] 0 GPa, 300 K values calculated using density functional theory.

$$C_V = \left(\frac{\partial U}{\partial T}\right)_V. \quad (9)$$

The molar heat capacity derived from the Debye model for internal energy (Eq. 3) is therefore:

$$C_V = 9nN_A k_B \left(\frac{T}{\theta_D}\right)^3 \int_0^{\theta_D/T} \frac{x^4}{\left[\exp(x)-1\right]^2} dx \quad (10)$$

where n is the number of atoms per formula unit and N_A is Avogadro's number. Equation 10 uses Debye theory and so at high-temperatures asymptotes to the classical limit $3Nk_B$, known as the Dulong-Petit law. The volumetric heat capacity (Eq. 10) can be obtained using the Debye temperatures calculated in the fit to the thermal expansion from Equations 4 and 7.

While this can sometimes be preferred, this limit does not take into account factors such as anharmonicity, or disordering (including defect formation), which are important because they

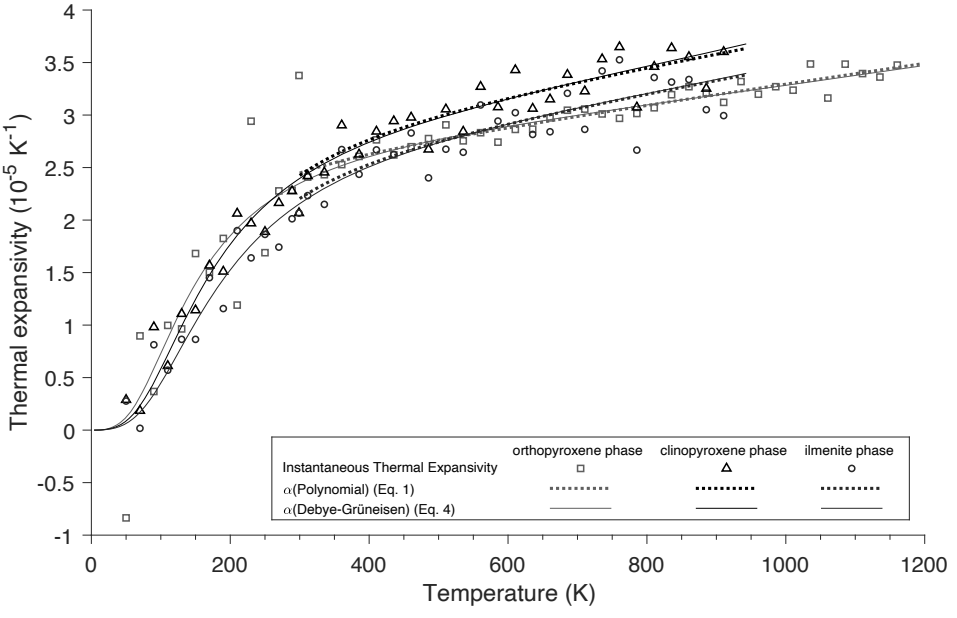

Figure 7. Volumetric thermal expansivity of $MgGeO_3$ phases. Lines and symbols as in the legend.

can raise the heat capacity of a material beyond the classical limit. Therefore, an alternative formulation of the heat capacity is to use the coefficient of thermal expansion, the thermodynamic Grüneisen parameter (γ_{th}) and the incompressibility (K) to calculate C_V as (Poirier 2000):

$$C_V = \alpha K V/\gamma_{th}. \quad (11)$$

This formulation contains no asymptotic limit and so may represent a more realistic model under high-temperature conditions. If it is again assumed that $\gamma_{th} = \gamma$ and that K is athermal (i.e., $K = K_0$), Equation 5 may be used to derive an expression for C_v without requiring the bulk modulus or a Grüneisen parameter:

$$C_V = \alpha V Q/V_0. \quad (12)$$

Neither value for C_v is directly comparable to experimental measurements of heat capacity that are made at constant pressure. The constant pressure or isobaric heat capacity (C_P) is related to the volumetric heat capacity as follows:

$$\left(\frac{C_P}{C_V}\right) = 1 + \gamma_{th}\alpha T. \quad (13)$$

Again, by assuming the Grüneisen parameters in Equations 5, 11, and 13 are the same C_P is calculable.

Figure 8 plots the calculated isobaric heat capacities for the three phases studied here along with previous data. At temperatures greater than ~300 K the heat capacities derived using Equation 12 become significantly greater than those from the simple Debye approximation (Eq. 10). Our calculated values for the heat capacity derived directly from the Debye model (i.e., via Eq. 10) are greater than the measured values of Ashida et al. (1985). At higher temperatures, though, the calculated heat capacities of Ross and Navrotsky (1988) are slightly smaller than our Debye-derived values at 298 K and are very close above 600 K. Below ~850 K, Ross and Navrotsky (1988) and our Debye heat capacities agree that C_P (clinopyroxene-structured $MgGeO_3$) > C_P (orthopyroxene-structured $MgGeO_3$) > C_P (ilmenite-structured $MgGeO_3$). The heat capacities derived from Equation 12 also have this condition below ~485 K. Above 635 K, these heat capacities have C_P (clinopyroxene-structured $MgGeO_3$) > C_P (ilmenite-structured $MgGeO_3$) > C_P (orthopyroxene-structured $MgGeO_3$), with the lower orthopyroxene phase heat capacity related to the smaller thermal expansion of the orthopyroxene phase relative to the other phases. This concords with the observations showing that, at <25 K in $MgSiO_3$, the heat capacity of clinopyroxene is greater than orthopyroxene (Drebushchak et al. 2008). It is clear from Figure 8 that the available experimental heat capacity data seem better matched by values we have obtained via Equation 10 and that the approximations inherent in Equation 12 may, therefore, be leading to an overestimate of P. However, Fiquet et al. (1992), have reported experimental values of C_P for other germanates at high temperature that exceed the value from the Dulong-Petit law by similar amounts to that shown in Figure 8, e.g., by up to 13% for olivine-structured Mg_2GeO_4 and 30% for olivine-structured $CaMgGeO_4$.

Thermodynamic Clapeyron slope

The Clapeyron slope of a phase boundary is given by:

$$dP/dT = \Delta S/\Delta V \quad (14)$$

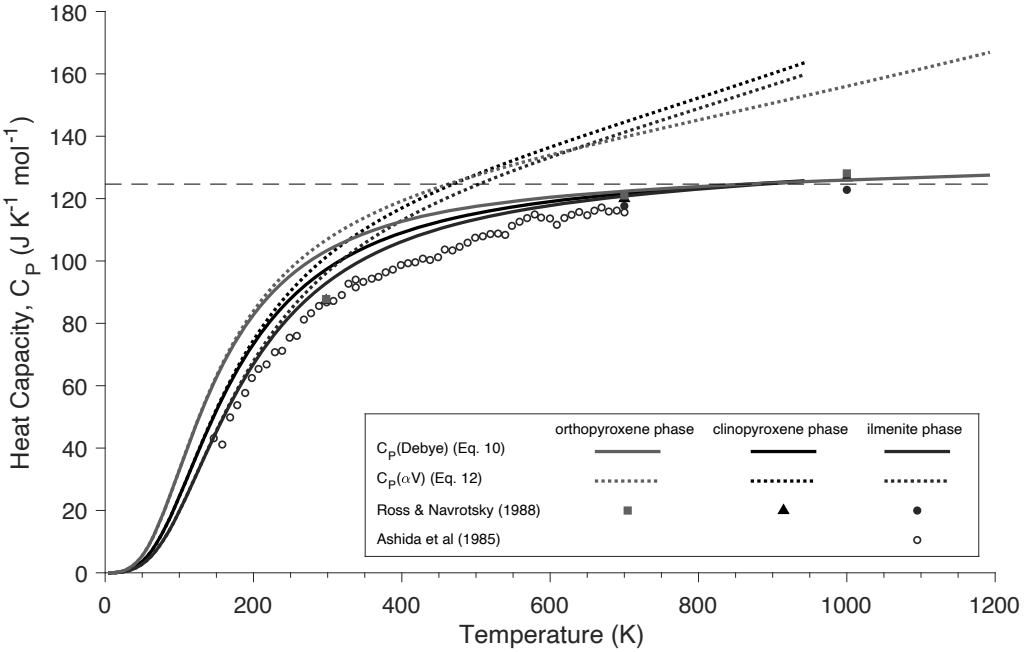

Figure 8. Calculated isobaric heat capacities of $MgGeO_3$ phases, converted from isovolumetric heat capacities (Eq. 13). Lines and symbols as in the legend. The horizontal dashed gray line is the Dulong-Petit limit for the heat capacity at constant volume.

where ΔS and ΔV are the entropy and volume change across the phase transition. The entropy of a mineral is related to its heat capacity by:

$$\left(\frac{\partial S}{\partial T}\right)_P = \frac{C_P}{T} \quad (15)$$

and, therefore, the thermophysical parameters calculated above are sufficient to estimate the Clapeyron slope of the boundary—provided that an adequate representation of C_P can be obtained from the thermal expansion measurements. For any set of isobaric measurements, the result will be the value of the Clapeyron slope as a function of temperature along the isobar. In the present work, the thermal expansion measurements have all been made at ambient pressure, and so the calculated slope will be that of the phase boundary at the point where it crosses the temperature axis in Figure 3. Thermodynamics requires that the Clapeyron slope must fall to zero as T approaches 0 K; for finite temperatures, in cases where the Clapeyron slope shows a strong temperature dependence, it then will be necessary to know the temperature of the phase boundary to calculate the correct value of the Clapeyron slope. As a result, the method described here provides only a check on the correctness of the slopes of phase boundaries, rather than a method for determining their absolute position in P-T space. The Clapeyron slopes, calculated using both representations of the heat capacities (Eqs. 10 and 12) for each phase transition, are plotted in Figure 9. The Clapeyron slopes at the 0 GPa intersection temperature are listed in Table 2.

Below ~300 K, there is little difference between Clapeyron slopes; however, they are calculated, but above this temperature the possible Clapeyron slopes show a wider range depending on the assumed heat capacity (Fig. 9). At high temperatures, Clapeyron slopes calculated with heat capacities directly from the Debye model (Eq. 10) show asymptotic behavior that is not present in Clapeyron slopes calculated using Equation 12. This is because the heat capacity from the Debye model asymptotes to the classical limit. With Debye-model heat capacities, the Clapeyron slope of the orthopyroxene-clinopyroxene phase boundary is always positive, but when Equation 12 is used, the Clapeyron slope is negative at temperatures greater than 1665 K (Fig. 9a). At 1736 K, where our orthopyroxene-clinopyroxene phase boundary intersects 0 GPa, the calculated Clapeyron slope is –1.8 MPa/K. For the clinopyroxene-ilmenite phase transition, the use of heat capacities obtained from Equation 12 increases the calculated Clapeyron slope, but it remains somewhat less than the experimental values of either Kirfel and Neuhaus (1974) or that found in the present work (Fig. 9b). However, when it is considered that these Clapeyron slopes are calculated from 0 GPa data and that there are several simplifying assumptions in the calculations, we believe that they strongly support the conclusion that our phase boundaries as determined by direct high-P/T experiments are correct.

Discussion

In this study, the experimental phase diagram is in excellent agreement with that of Kirfel and Neuhaus (1974). Both studies find a negative Clapeyron slope for the orthopyroxene-clinopyroxene phase boundary and the orthopyroxene-clinopyroxene-ilmenite phase triple point close to 0.98 GPa and 752 K. This topology is different from the $MgSiO_3$ system, in which the Clapeyron slope of the orthopyroxene-clinopyroxene transition is positive and there is no equivalent triple point. There is no evidence for a low-temperature $P2_1/c$ clinopyroxene-structured $MgGeO_3$ phase and it is not required by the phase diagram. However, it may be kinetically inhibited from forming below ~900 K but this seems unlikely given that in $MgSiO_3$ the $P2_1/c$ clinopyroxene forms spontaneously during decompression of the $C2/c$ clinopyroxene. The phase diagram is also consistent with orthopyroxene-structured $MgGeO_3$ transforming directly to the $C2/c$ clinopyroxene phase above 1828 K at 0 GPa. There is no significant break in slope of the orthopyroxene-clinopyroxene phase boundary (Fig. 1a) that may indicate the presence of the protopyroxene (*Pbcn*) structure argued for by Ozima and Akimoto (1983). Although its presence cannot be excluded, if it does exist, it is likely to have only a small narrow, high temperature, stability field.

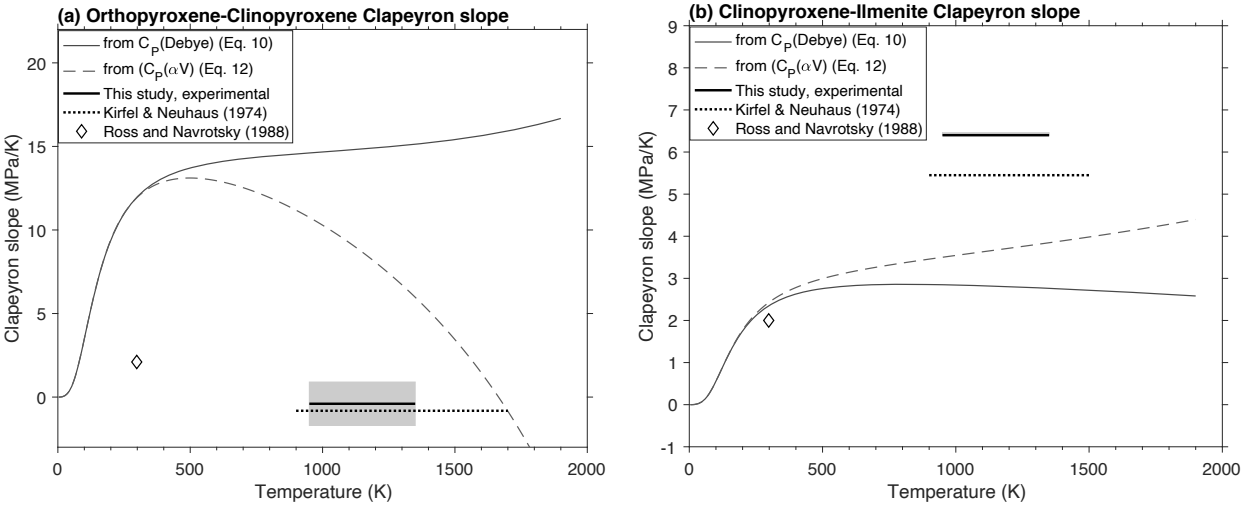

Figure 9. Clapeyron slopes of the (**a**) orthopyroxene-clinopyroxene and (**b**) clinopyroxene-ilmenite phase transitions. Lines and symbols as in the legends.

Our experimental phase diagram, and that of Kirfel and Neuhaus (1974), are consistent with the thermophysical property measurements if the heat capacity exceeds the Dulong-Petit limit (Eq. 12). In this case, the heat capacity estimated for the clinopyroxene phase increases faster than that of the orthopyroxene phase (Fig. 8). The associated relative increase in the entropy of the clinopyroxene phase at high temperatures changes the Clapeyron slope (Eq. 14), expanding the phase field at the expense of the orthopyroxene phase. Although the heat capacity of ilmenite-structured $MgGeO_3$ (Fig. 8) is consistent with the Dulong-Petit limit, and would thus have negligible anharmonicity, assuming heat capacities calculated using Equation 12 leads to Clapeyron slopes that correspond better to the phase boundaries determined by direct experiment. There are no measurements of heat capacity in germanate pyroxenes with which we can compare our estimates, but heat capacities well above the Dulong-Petit limit have been observed in germanate olivines (Fiquet et al. 1992) and significant anharmonicity has been observed in germanate perovskites (Andrault et al. 2015). The prevalence of anharmonicity more generally in germanate oxides points to it being present in the phases here and the cause of their apparently increased heat capacity. We note, though, that other processes can cause increases in heat capacity at high temperature, e.g., defect formation (Pamato et al. 2018).

Whatever is assumed about the heat capacity, for the clinopyroxene-ilmenite phase transition, our results are in broad agreement with those of Ross and Navrotsky (1988). Our phase diagram and interpretation of the thermophysical properties, though, disagrees with their results for the orthopyroxene-clinopyroxene phase boundary.

Although anharmonicity and/or significant formation of defects in clinopyroxene-structured $MgGeO_3$ can reconcile the experimental observations, there is another factor that may explain the discrepancies, between studies, namely an extremely small transformation shear-stress between clinopyroxene and orthopyroxene-structured phases. The possibility that the low-pressure extent of the clinopyroxene phase field is controlled by shear-stress controlled back-transformation has been presented before (Ringwood and Seabrook 1962) and has been observed during deformation of natural pyroxenes (Coe and Kirby 1975). It is unlikely, though, that this effect has any effect on the phase diagram here because: (1) our phase boundary is in almost perfect agreement with that of Kirfel and Neuhaus (1974), and (2) the clinopyroxene-structured $MgGeO_3$ samples were ground prior to the thermal expansion measurements and no back transformation was observed in the sample.

Implications

Based on the evidence in this study, we suggest that $MgGeO_3$ polymorphs and the clinopyroxene in particular may be significantly more anharmonic than the equivalent $MgSiO_3$ polymorphs. This observation unifies the experimental observations of the phase boundaries; however, there are currently no heat capacity measurements against which to test this assertion. Therefore, to fully understand the system, more thermophysical property measurements and/or in situ experiments must be performed.

The presence of potentially significant anharmonicity in clinopyroxene-structured $MgGeO_3$, magnesium germanates (e.g., Fiquet et al. 1992) and germanates more generally (e.g., Andrault et al. 1996), is a major difference between the germanate and silicate systems. These effects must therefore be considered when using germanates as low-pressure analogs for Earth-forming minerals, especially at elevated temperatures.

Acknowledgments and Funding

S.A.H. (NE/L006898/1, NE/P017525/1), J.R.S., and D.P.D. (NE/K002902/1) thank the Natural Environment Research Council for funding. I.G.W. thanks the Science and Technology Facilities Council (ST/K000934/1) for funding. This work is based on the Ph.D. thesis work of J.R.S. (University College London 2017).

References cited

Akaogi, M., Ito, E., and Navrotsky, A. (1989) Olivine-modified spinel-spinel transitions in the system Mg_2SiO_4-Fe_2SiO_4: Calorimetric measurements, thermochemical calculation, and geophysical application. Journal of Geophysical Research: Solid Earth, 94, 15,671–15,685.

Akaogi, M., Kojitani, H., Yusa, H., Yamamoto, R., Kido, M., and Koyama, K. (2005) High-pressure transitions and thermochemistry of $MGeO_3$ (M=Mg, Zn and Sr) and Sr-silicates: Systematics in enthalpies of formation of $A^{2+}B^{4+}O^3$ perovskites. Physics and Chemistry of Minerals, 32, 603–613.

Andrault, D., Itié, J.P., and Farges, F. (1996) High-temperature structural study of germanate perovskites and pyroxenoids. American Mineralogist, 81 (7-8), 822–832.

Angel, R.J., and Hugh-Jones, D.A. (1994) Equations of state and thermodynamic properties of enstatite pyroxenes. Journal of Geophysical Research, 99, 777–783.

Angel, R.J., and Jackson, J.M. (2002) Elasticity and equation of state of orthoenstatite, $MgSiO_3$. American Mineralogist, 87, 558–561.

Ashida, T., Miyamoto, Y., and Kume, S. (1985) Heat capacity, compressibility and thermal expansion coefficient of ilmenite-type $MgGeO_3$. Physics and Chemistry of Minerals, 12, 129–131.

Boyd, F.R., and England, J.L. (1960) Apparatus for phase-equilibrium measurements at pressures up to 50 kilobars and temperatures up to 1750 °C. Journal of Geophysical Research, 65, 741.

Coe, R.S., and Kirby, S.H. (1975) The orthoenstatite to clinoenstatite transformation by shearing and reversion by annealing: Mechanism and potential applications. Contributions to Mineralogy and Petrology, 52, 29–55.

Drebushchak, V.A., Kovalevskaya, Y.A., Paukov, I.E., and Surkov, N.V. (2008) Low-temperature heat capacity of monoclinic enstatite. Journal of Thermal Analysis and Calorimetry, 94, 493–497.

Reference is:

Fei, Y. (1995) Thermal expansion. In T.J. Ahrens, Ed., Mineral Physics & Crystallography, https://doi.org/10.1029/RF002p0029.

Fiquet, G., Gillet, P., and Richet, P. (1992) Anharmonicity and high-temperature heat capacity of crystals: The examples of Ca_2GeO_4, Mg_2GeO_4, and $CaMgGeO_4$ olivines. Physics and Chemistry of Minerals, 18, 469–479.

Hirose, K., Kawamura, K., Ohishi, Y., Tateno, S., and Sata, N. (2005) Stability and equation of state of $MgGeO_3$ post-perovskite phase. American Mineralogist, 90, 262–265.

Hölzer, G., Fritsch, M., Deutsch, M., Härtwig, J., and Förster, E. (1997) $K\alpha_{1,2}$ and $K\beta_{1,3}$ X-ray emission lines of the 3*d* transition metals. Physical Review A, 56, 4554–4568.

Hugh-Jones, D. (1997) Thermal expansion of $MgSiO_3$ and $FeSiO_3$ ortho- and clinopyroxenes. American Mineralogist, 82, 689–696.

Hunt, S.A., Wann, E.T.H., Dobson, D.P., Vočadlo, L., and Wood, I.G. (2017) The thermal expansion of $(Fe_{1-y}Ni_y)Si$. Journal of Physics: Condensed Matter, 29, 335701.

Ito, E., and Matsui, Y. (1979) High-pressure transformations in silicates, germanates, and titanates with ABO_3 stoichiometry. Physics and Chemistry of Minerals, 4, 265–273.

Kirfel, A., and Neuhaus, A. (1974) Zustandsverhalten und elektrische Leitfähigkeit von $MgGeO_3$ bei Drücken bis 65 kbar und Temperaturen bis 1300 °C (mit Folgerungen für das Druckverhalten von $MgSiO_3$). Zeitschrift für Physikalische Chemie, 91, 121–152.

Kirfel, A., Hinze, E., and Will, G. (1978) The rhombohedral high pressure phase of $MgGeO_3$ (ilmenite): Synthesis and single crystal structure analysis. Zeitschrift für Kristallographie—New Crystal Structures, 148, 305–317.

Knight, K.S., and Price, G.D. (2008) Powder neutron-diffraction studies of clinopyroxenes. I. The crystal structure and thermoelastic properties of jadeite between 1.5 and 270 K. Canadian Mineralogist, 46, 1593–1622.

Knittle, E. (1995) Static compression measurements of equations of state. In T.J. Ahrens, Ed., Mineral Physics and Crystallography: A handbook of physical constants, vol. 2 pp. 98–142. American Geophysics Union.

Kostiner, E., and Bless, P.W. (1971) Magnesium germanate and fluorogermanate. Journal of the Electrochemical Society, 118, 351.

Larson, A.C., and Von Dreele, R.B. (2000) General Structure Analysis System. Report LAUR 86-748.
Laubengayer, A.W., and Morton, D.S. (1932) Germanium. XXXIX. The polymorphism of germanium dioxide 1. Journal of the American Chemical Society, 54, 2303–2320.
Le Bail, A., Duroy, H., and Fourquet, J.L. (1988) Ab-initio structure determination of $LiSbWO_6$ by X-ray powder diffraction. Materials Research Bulletin, 23, 447–452.
Leinenweber, K., Wang, Y., Yagi, T., and Yusa, H. (1994) An unquenchable perovskite phase of $MgGeO_3$ and comparison with $MgSiO_3$ perovskite. American Mineralogist, 79, 197–199.
Liebermann, R.C. (1974) Elasticity of pyroxene-garnet and pyroxene-ilmenite phase transformations in germanates. Physics of the Earth and Planetary Interiors, 8, 361–374.
Lindemann, W. (1961) The unit cell and space group of $MgGeO_3$. Acta Crystallographica, 14, 998–998.
Lindsay-Scott, A., Wood, I.G., and Dobson, D.P. (2007) Thermal expansion of $CaIrO_3$ determined by X-ray powder diffraction. Physics of the Earth and Planetary Interiors, 162, 140–148.
Lyon, S.R. (1968) Phase reactions in the systems MgO-SiO_2-MgF_2, MgO-GeO_2-MgF_2, and MgO-GeO_2-$Mg(OH)_2$. Ph.D. thesis, Ohio State University.
McCormick, G.R. (1964) An investigation of the compatibility relations in the system MgO-GeO-MgF_2-LiF principally at 1000 °C. Ohio State University.
Murakami, T., Takeuchi, Y., and Yamanaka, T. (1982) The transition of orthoenstatite to protoenstatite and the structure at 1080 °C. Zeitschrift für Kristallographie—New Crystal Structures, 160, 299–312.
Oganov, A.R., and Dorogokupets, P.I. (2004) Intrinsic anharmonicity in equations of state and thermodynamics of solids. Journal of Physics Condensed Matter, 16, 1351–1360.
Ohi, S., and Miyake, A. (2016) Phase transitions between high- and low-temperature orthopyroxene in the $Mg_2Si_2O_6$-$Fe_2Si_2O_6$ system. American Mineralogist, 101, 1414–1422.
Okada, T., Narita, T., Nagai, T., and Yamanaka, T. (2008) Comparative Raman spectroscopic study on ilmenite-type $MgSiO_3$ (akimotoite), $MgGeO_3$, and $MgTiO_3$ (geikielite) at high temperatures and high pressures. American Mineralogist, 93, 39–47.
Ozima, M. (1983) Structure of orthopyroxene-type and clinopyroxene-type magnesium germanium oxide $MgGeO_3$. Acta Crystallographica, C39, 1169–1172.
Ozima, M., and Akimoto, S.I. (1983) Flux growth of single crystals of $MgGeO_3$ polymorphs (orthopyroxene, clinopyroxene, and ilmenite) and their phase relations and crystal structures. American Mineralogist, 68, 1199–1205.
Pamato, M.G., Wood, I.G., Dobson, D.P., Hunt, S.A., and Vočadlo, L. (2018) The thermal expansion of gold: Point defect concentrations and pre-melting in a face-centred cubic metal. Journal of Applied Crystallography, 51, 470–480.
Poirier, J.-P. (2000) Introduction to the Physics of the Earth's Interior. Cambridge University Press.
Redhammer, G.J., Senyshyn, A., Tippelt, G., Pietzonka, C., Roth, G., and Amthauer, G. (2010a) Magnetic and nuclear structure and thermal expansion of orthorhombic and monoclinic polymorphs of $CoGeO_3$ pyroxene. Physics and Chemistry of Minerals, 37, 311–332.
Redhammer, G.J., Cámara, F., Alvaro, M., Nestola, F., Tippelt, G., Prinz, S., Simons, J., Roth, G., and Amthauer, G. (2010b) Thermal expansion and high-temperature $P2_1/c$-$C2/c$ phase transition in clinopyroxene-type $LiFeGe_2O_6$ and comparison to $NaFe(Si,Ge)_2O_6$. Physics and Chemistry of Minerals, 37, 685–704.
Rietveld, H.M. (1969) A profile refinement method for nuclear and magnetic structures. Journal of Applied Crystallography, 2, 65–71.
Ringwood, A.E., and Seabrook, M. (1962) High-pressure transition of $MgGeO_3$ from pyroxene to corundum structure. Journal of Geophysical Research, 67, 1690–1691.
Robbins, C.R., and Levin, E.M. (1959) The system magnesium oxide-germanium dioxide. American Journal of Science, 257(1), 63–70.
Ross, N.L., and Navrotsky, A. (1987) The Mg_2GeO_4 olivine-spinel phase transition. Physics and Chemistry of Minerals, 14, 473–481.
——— (1988) Study of the $MgGeO_3$ polymorphs (orthopyroxene, clinopyroxene, and ilmenite structures) by calorimetry, spectroscopy, and phase equilibria. American Mineralogist, 73, 1355–1365.
Roth, R.S. (1955) Synthetic alkaline earth germanates isostructural with enstatite and pseudowollastonite. American Mineralogist, 40, 322.
——— (1957) Classification of perovskite and other ABO_3-type compounds. Journal of Research of the National Bureau of Standards, 58, 75.
Sarver, J.F., and Hummel, F.A. (1963) Subsolidus equilibria and luminescence data on phases in the system MgO-GeO_2-SiO_2-TiO_2. Journal of the Electrochemical Society, 110, 726.
Sato, Y., Ito, E., and Akimoto, S.-i. (1977) Hydrostatic compression of ilmenite phase of $ZnSiO_3$ and $MgGeO_3$. Physics and Chemistry of Minerals, 2, 171–176.
Thompson, P., and Wood, I.G. (1983) X-ray Rietveld refinement using Debye-Scherrer geometry. Journal of Applied Crystallography, 16, 458–472.
Toby, B.H. (2001) EXPGUI, a graphical user interface for GSAS. Journal of Applied Crystallography, 34, 210–213.
Tsuchiya, T., and Tsuchiya, J. (2007) High-pressure-high-temperature phase relations of $MgGeO_3$: First-principles calculations. Physical Review B: Condensed Matter and Materials Physics, 76, 2–5.
Ulmer, P., and Stalder, R. (2001) The Mg(Fe)SiO_3 orthoenstatite-clinoenstatite transitions at high pressures and temperatures determined by Raman-spectroscopy on quenched samples. American Mineralogist, 86, 1267–1274.
Vegard, L. (1932) Die Struktur von β-Stickstoff und die verschiedene Phosphoreszenzfähigkeit der beiden Formen des festen Stickstoffs. Zeitschrift für Physik, 79, 471–491.
Vočadlo, L., Knight, K.S., Price, G.D., and Wood, I.G. (2002) Thermal expansion and crystal structure of FeSi between 4 and 1173 K determined by time-of-flight neutron powder diffraction. Physics and Chemistry of Minerals, 29, 132–139.
von Dreele, R.B., Bless, P.W., Kostiner, E., and Hughes, R.E. (1970) The crystal structure of magnesium germanate: A reformulation of Mg_4GeO_6 as $Mg_{28}Ge_{10}O_{48}$. Journal of Solid State Chemistry, 2, 612–618.
Walker, D., Carpenter, M.A., and Hitch, C.M. (1990) Some simplifications to multianvil devices for high pressure experiments. American Mineralogist, 75, 1020–1028.
Wallace, D.C. (1998) Thermodynamics of Crystals. Dover Publications.
Wood, I.G., Dominic Fortes, A., Dobson, D.P., Wang, W., Pajdzik, L., and Cosier, J. (2018) Investigation of high-pressure planetary ices by cryo-recovery. I. an apparatus for X-ray powder diffraction from 40 to 315 K, allowing 'cold loading' of samples. Journal of Applied Crystallography, 51, 685–691.
Yamanaka, T., Hirano, M., and Takeuchi, Y. (1985) A high temperature transition in $MgGeO_3$ from clinopyroxene ($C2/c$) type to orthopyroxene (*Pbca*) type. American Mineralogist, 70, 365–374.
Yamanaka, T., Komatsu, Y., Sugahara, M., and Nagai, T. (2005) Structure change of $MgSiO_3$, $MgGeO_3$, and $MgTiO_3$ ilmenites under compression. American Mineralogist, 90, 1301–1307.
Yang, H., and Ghose, S. (1994) Thermal expansion, Debye temperature and Grüneisen parameter of synthetic (Fe, Mg)SiO_3 orthopyroxenes. Physics and Chemistry of Minerals, 20, 575–586.

Manuscript received June 26, 2020
Manuscript accepted December 4, 2020
Manuscript handled by Jennifer Kung